Access to this work was provided by the University of Maryland, Baltimore County (UMBC) ScholarWorks@UMBC digital repository on the Maryland Shared Open Access (MD-SOAR) platform.

Please provide feedback

Please support the ScholarWorks@UMBC repository by emailing scholarworks-group@umbc.edu and telling us what having access to this work means to you and why it's important to you. Thank you.

The Luminosity Phase Space of Galactic and Extragalactic X-ray Transients Out to Intermediate Redshifts

AVA POLZIN [ID],[1] RAFFAELLA MARGUTTI [ID],[2,3] DEANNE COPPEJANS [ID],[4,5] KATIE AUCHETTL [ID],[6,7,8] KIM L. PAGE [ID],[9] GEORGIOS VASILOPOULOS [ID],[10,11] JOE S. BRIGHT [ID],[12] PAOLO ESPOSITO [ID],[13,14] PETER K. G. WILLIAMS [ID],[15,16] KOJI MUKAI [ID],[17,18] AND EDO BERGER [ID][15]

[1]Department of Astronomy and Astrophysics, The University of Chicago, Chicago, IL 60637, USA.
[2]Department of Astronomy, University of California, Berkeley, CA, 94720
[3]Department of Physics, University of California, Berkeley, CA, 94720
[4]Department of Physics, University of Warwick, Gibbet Hill Road, Coventry CV4 7AL, UK
[5]Department of Physics & Astronomy and Center for Interdisciplinary Exploration and Research in Astrophysics, Northwestern University, Evanston, IL, 60208
[6]School of Physics, The University of Melbourne, Parkville, VIC 3010, Australia
[7]ARC Centre of Excellence for All Sky Astrophysics in 3 Dimensions (ASTRO 3D)
[8]Department of Astronomy and Astrophysics, University of California, Santa Cruz, CA 95064, USA
[9]School of Physics & Astronomy, University of Leicester, Leicester LE1 7RH, UK
[10]Université de Strasbourg, CNRS, Observatoire astronomique de Strasbourg, UMR 7550, F-67000 Strasbourg, France
[11]Department of Astronomy, Yale University, New Haven, CT 06511
[12]Astrophysics, Department of Physics, University of Oxford, Keble Road, Oxford OX1 3RH, UK
[13]Scuola Universitaria Superiore IUSS Pavia, Palazzo del Broletto, piazza della Vittoria 15, 27100 Pavia, Italy
[14]INAF–Istituto di Astrofisica Spaziale e Fisica Cosmica di Milano, Via A. Corti 12, 20133 Milano, Italy
[15]Center for Astrophysics | Harvard & Smithsonian, 60 Garden Street, Cambridge, MA 02138-1516, USA
[16]American Astronomical Society, 1667 K Street NW, Suite 800, Washington, DC, 20006, USA
[17]CRESST II and X-ray Astrophysics Laboratory, NASA/GSFC, Greenbelt, MD 20771, USA
[18]Department of Physics, University of Maryland, Baltimore County, 1000 Hilltop Circle, Baltimore, MD 21250, USA

ABSTRACT

We present a detailed compilation and analysis of the X-ray phase space of low- to intermediate-redshift transients that consolidates observed light curves (and theory where necessary) for a large variety of classes of transient/variable phenomena in the 0.3–10 keV band including gamma-ray burst afterglows, supernovae, supernova shocks interacting with the environment, tidal disruption events and active galactic nuclei, fast blue optical transients, cataclysmic variables, magnetar flares/outbursts and fast radio bursts, cool stellar flares, X-ray binary outbursts, and ultraluminous X-ray sources. Our over-arching goal is to offer a comprehensive resource for the examination of these ephemeral events, extending the X-ray duration-luminosity phase space (DLPS) to show luminosity evolution. We use existing observations (both targeted and serendipitous) to characterize the behavior of various transient/variable populations. Contextualizing transient signals in the larger DLPS serves two primary purposes: to identify areas of interest (i.e., regions in the parameter space where one would expect detections, but in which observations have historically been lacking) and to provide initial qualitative guidance in classifying newly discovered transient signals. We find that while the most luminous (largely extragalactic) and least luminous (largely Galactic) part of the phase space is well-populated at $t > 0.1$ days, intermediate luminosity phenomena ($L_x = 10^{34} - 10^{42}$ erg s^{-1}) represent a gap in the phase space. We thus identify $L_x = 10^{34} - 10^{42}$ erg s^{-1} and $t = 10^{-4} - 0.1$ days as a key discovery phase space in transient X-ray astronomy.

Corresponding author: Ava Polzin
apolzin@uchicago.edu

1. INTRODUCTION

Transient and variable electromagnetic emission is often associated with the most violent events in space, like stellar explosions, stellar disruptions by supermassive black holes, or accretion-related phenomena on compact objects to name a few. Studying the timescales and intrinsic energy released by each of these phenomena often provide guidance to understand the physics that regulates the bright displays of these transients and variables. To this end, the duration-luminosity phase space (DLPS) has been used as a means of placing classes of transient and variable phenomena in the context of their underlying physics and constraining their outburst mechanisms.

Previous works have focused on building an observationally motivated, light curve-populated DLPS for specific wavelength regimes (e.g., Kulkarni 2012; Pietka et al. 2015; Villar et al. 2017 for optical wavelengths, Eftekhari et al. 2022 for millimeter wavelengths, or Metzger et al. 2015 for radio wavelengths), which is facilitated by the significant volume of available data. We build on the first attempts to produce an observation-driven DLPS in the X-rays (Soderberg et al. 2009; O'Brien & Smartt 2013) by populating the DLPS with light curves as a comprehensive view of the low- to intermediate-redshift ($z \leq 1$) phase space for (observer frame) 0.3-10 keV transient and variable X-ray phenomena. This extends the use of the DLPS by showing both luminosity and time evolution of these events. The motivation behind compiling this dataset is two-pronged: to identify pristine regions of this parameter space that can be explored by future observing facilties (i.e., identification of discovery areas) and conversely, we can use the phase space location of an unknown type of transient to constrain its intrinsic nature. This dual motivation, both for characterizing the nature of observed events and for identifying discovery frontiers for the future generation of X-ray observatories, make examination of the phase space vital.

We utilize complete light curves for a variety of Galactic and extragalactic transient and variable phenomena: gamma-ray burst afterglows, supernovae, supernova shocks interacting with the environment, tidal disruption events and active galactic nuclei, fast blue optical transients, cataclysmic variables, magnetar flares/outbursts and fast radio bursts, cool stellar flares, X-ray binary outbursts, and ultraluminous X-ray sources. For some classes the data are sparse, and we

will instead plot peak X-ray luminosity (L_x) vs. duration. In the one case where there were insufficient (*confirmed*) observations, we used theory as a supplement.

We present in Section 2 the datasets for each of the different classes of transient and variable events, and we discuss their location within the DLPS. In Section 3, we examine the use cases for our comprehensive DLPS (Figures 1 and 2). Where available, redshifts were used to correct the duration to the rest frame as well as to determine the luminosity distance, assuming a cosmology with $H_0 = 69.6$ km s^{-1} Mpc^{-1}, $\Omega_M = 0.286$, and $\Omega_\Lambda = 0.714$.

2. DATA

We assembled X-ray data from a variety of sources. For ease and readability, we include lists of events, as well as their classifications, coordinates, distances, and the relevant literature in Appendix A. Light curve data used in this paper are available on GitHub[1].

2.1. *Gamma-ray Burst (GRB) Afterglows*

Gamma-Ray Bursts (GRBs) are burst of γ-rays associated with either the collapse of a massive star (GRBs with a duration of the γ-ray emission $T_{90} > 2$ s) or the merger of compact objects (i.e. neutron stars and black holes). All GRB X-ray afterglow data shown in Figure 3 were collected via the UK *Swift* Science Data Centre[2] (Evans et al. 2007, 2009), with the notable exceptions of the pre-*Swift* era subluminous GRBs, GRB980425A (Pian et al. 2000; Kouveliotou et al. 2004) and GRB031203A (Sazonov et al. 2004; Watson et al. 2004). We include long GRBs, short GRBs, ultralong GRBs, and subluminous GRBs in our plotted population where redshift information is available[3] and $z \leq 1$. We also include the X-ray afterglow counterpart of the neutron-star merger event GW170817, for which gravitational-wave emission was detected (e.g., Abbott et al. 2017; Hajela et al. 2019, 2020; Nakar 2020; Margutti & Chornock 2021). We excluded GRBs without well-constrained redshifts as we are interested in luminosity vs. intrinsic duration (rather than fluence vs. observed duration).

---

[1] https://github.com/avapolzin/X-rayLCs – this repository will be made public once the paper is accepted.

[2] https://www.swift.ac.uk

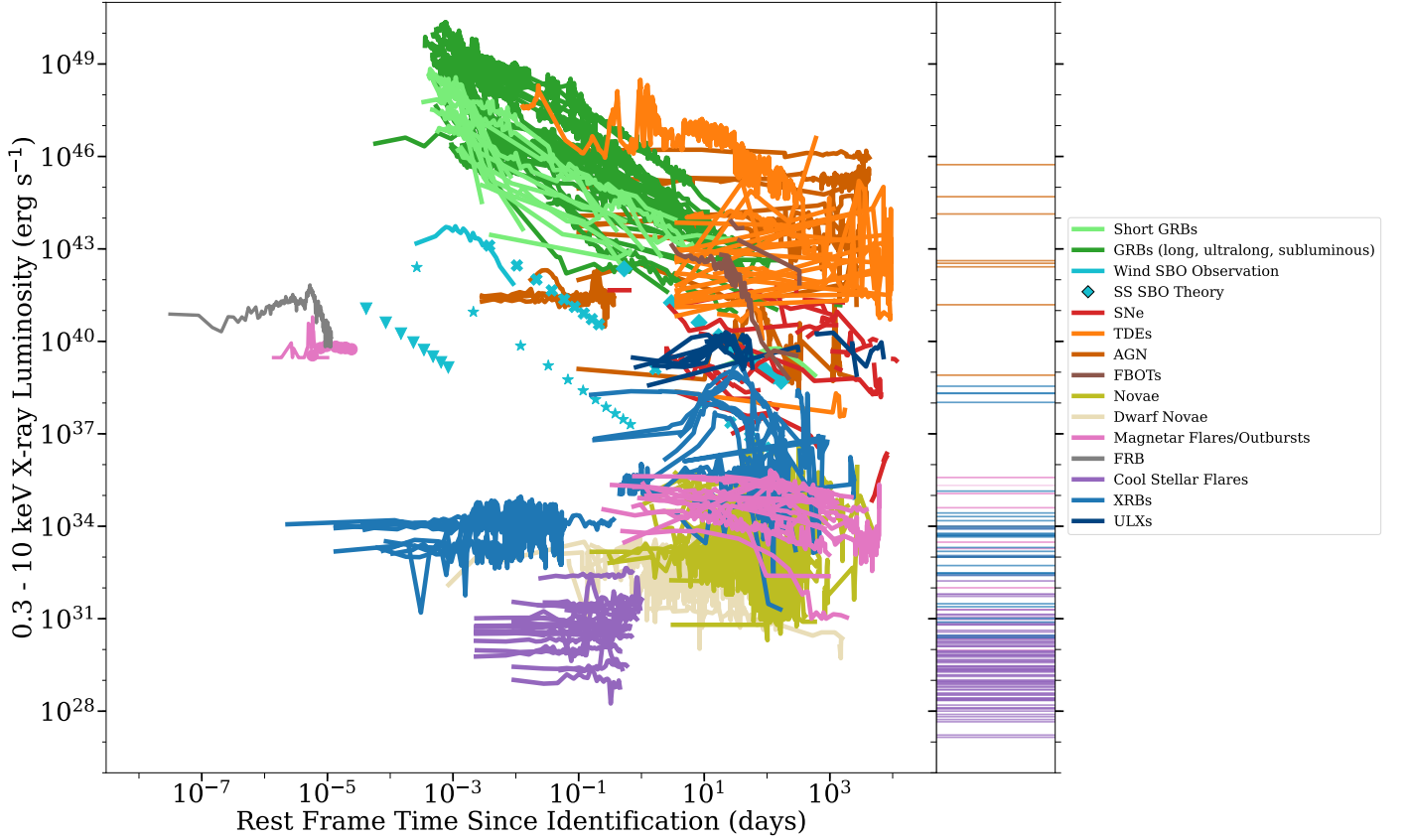[3] http://www.mpe.mpg.de/∼jcg/grbgen.html

Figure 1. X-ray phase space of transients and variable phenomena, including gamma-ray burst (GRB) afterglows, supernovae (SNe), supernova shock breakouts (SBOs), tidal disruption events (TDEs) and active galactic nuclei (AGN), fast blue optical transients (FBOTs), cataclysmic variables, magnetar flares/outbursts and fast radio bursts, cool stellar flares, X-ray binary outbursts, and ultraluminous X-ray sources. *Main Panel*: X-ray luminosity evolution with rest-frame time since identification. Theoretical SBO peak L_x-duration points are shown with different symbols corresponding to the model's input parameters; see Section 2.2 for details. *Right Side Panel:* To offer a sense of their persistent behavior, the quiescent luminosities of the included variable classes (AGN, magnetar flares/outbursts, M-dwarf flares, X-ray binaries, and ultraluminous X-ray sources) are shown as horizontal bars.

Differentiation of the sub-classes of GRBs was informed by the T_{90} parameter (i.e. the time interval over which 90% of the γ-ray emission is observed). Short GRBs typically have $T_{90} < 2\,$s, long GRBs fall within the $2 - 10^3\,$s range (Kouveliotou et al. 1993), and ultralong GRBs have T_{90} between $10^3 - 10^4\,$s (Levan et al. 2014). We note that some subluminous GRBs, while having a duration similar to that of long or ultralong GRBs, might actually represent physically distinct phenomena (e.g. supernova shock breakouts see Section 2.2).

2.2. *Explosion Shock Breakouts*

Shock breakouts (SBOs) are the emergence of the first (observable) photons from a stellar explosion. A SBO occurs as the shock goes through the star and reaches an optical depth of $\tau \sim c/v_{\rm shock}$ within the star or at the stellar surface or in the stellar wind. Short-duration energetic emission is observable in the X-rays if the shock breaks out from a compact progenitor (Nakar & Sari

2010). SBOs are short duration when their emission peaks in the X-rays, and there is only one broadly accepted observation (Soderberg et al. 2008, see however Mazzali et al. 2008 for a different interpretation), which was a serendipitous detection from a normal type Ib supernova, SN 2008D. While searches of archival data yield potential SBO candidates (e.g. Alp & Larsson 2020; Novara et al. 2020), wide-field X-ray instruments are vital for growing the sample of SBO observations. We note that later analysis of the prompt X-ray signal at the location of SN 2008D showed what is thought to be a breakout from the stellar wind (Balberg & Loeb 2011; Svirski & Nakar 2014). We tentatively include subluminous GRBs as candidate stellar surface breakouts associated with energetic type Ic-BL supernovae in Figure 3.

In order to better populate the X-ray phase space (Figure 3), we supplement the proposed stellar surface SBO light curves (from subluminous GRBs) with results
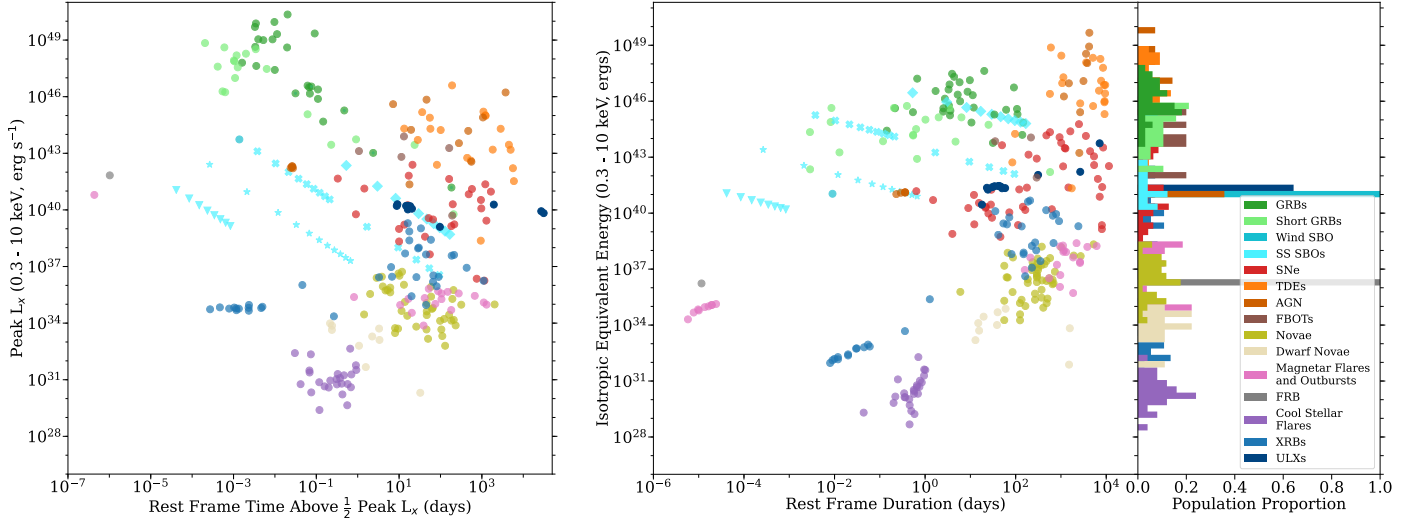
Figure 2. *Left Panel:* The peak X-ray luminosity vs. time above half-maximum light. *Right Panel:* At left, the overall energy released during the event vs. the duration of the transient event, and at right, the distribution of isotropic equivalent energies released for each class of transient/variable. As in Figure 1, theoretical SBO peak L_x-duration point markers correspond to different input parameters in the model.

from theoretical calculations by Nakar & Sari (2012). These authors show that:

$$E_{bo} \approx 6 \times 10^{46}\, E_{53}^{2.3} M_{ej,5}^{-1.65} R_5^{0.7}\ \mathrm{erg} \tag{1}$$

$$T_{bo} \approx 700\, E_{53}^{1.7} M_{ej,5}^{-1.2} R_5^{-0.95}\ \mathrm{keV} \tag{2}$$

$$t_{bo}^{obs} \approx 0.06\, E_{53}^{-3.4} M_{ej,5}^{2.5} R_5^{2.9}\ \mathrm{s} \tag{3}$$

$$L_{bo} \approx 4 \times 10^{47}\, E_{53}^{5.1} M_{ej,5}^{-3.65} R_5^{-1.85}\ \mathrm{erg\ s^{-1}} \tag{4}$$

Where E_{bo}, T_{bo}, t_{bo}^{obs}, and L_{bo} refer to the breakout energy, temperature, observed time (duration), and luminosity respectively. E_{53} is energy in terms of 10^{53} erg, $M_{ej,5}$ is the ejecta mass in terms of $5M_\odot$, and R_5 is the stellar radius in terms of $5R_\odot$.

We use a grid of energy values (between 10^{51} and 10^{52} erg), ejecta mass (between 1 and $10M_\odot$), and stellar radius (between 10^{10} and 10^{13} cm, which span the properties of Wolf-Rayet stars to red supergiants) to compute E_{bo}, T_{bo}, t_{bo}, and L_{bo} from Equations 1 - 4. Though a red supergiant with a breakout energy of 10^{52} erg is a less likely physical scenario, we include it anyway to account for the full range of possible progenitors that give rise to SBOs within the phase space. Similarly, in order to populate the phase space with potential durations vs. peak luminosities, we limit our plotted sample to those with temperatures (from Equation 2) in the range 0.1-20 keV as representative of the SBOs that will have some X-ray luminosity component in the 0.3-10 keV range of interest. In the upper-right panel of Figure 3, each individual point represents the peak luminosity and duration of a single theoretical stellar surface SBO event.

2.3. *Supernovae*

Supernova (SN) shocks that propagate in the explosion's environment are well-known particle accelerators and well-known sources of X-ray emission as the shocks decelerate and the particles cool down (e.g., Chevalier & Fransson 2017 for a recent review). We collected X-ray data for supernovae from a variety of sources (see Appendix A for details). Because of the rather limited sample of existing observations, we include all available ($z \leq 1$) X-ray light curves in bands with lower energy limits between 0.2 and 0.5 keV and upper energy limits between 8 and 12 keV, which are then k-corrected to the observed 0.3-10 keV band assuming a spectrum $F_\nu \propto \nu^{-\beta}$ with a spectral index $\beta = 1$ (equivalent to a photon index $\Gamma = 2$). These k-corrected data are shown in Figure 3.

We divide the SNe into three sub-classes based on their underlying physical properties: *Type I core-collapse* to be comprised of Type Ib, Ic, Ib/c, Ic/pec, and IIb SNe; *Type II core-collapse* to be comprised of Type II, IIP, IIL, and IIpec SNe; and *Interacting SNe* (i.e. SNe with signatures of CSM interaction in their optical spectra) to be comprised of Type IIn, Ibn, and Ia-CSM SNe. Additionally, we designate (optically) *superluminous SNe* and *Ca-rich SNe* separately as the two sub-classes of SNe for which X-ray emission has been most recently found.

2.4. *Tidal Disruption Events and Active Galactic Nuclei*

Tidal disruption events (TDEs) occur when a star passes close enough to a black hole that stellar mate-
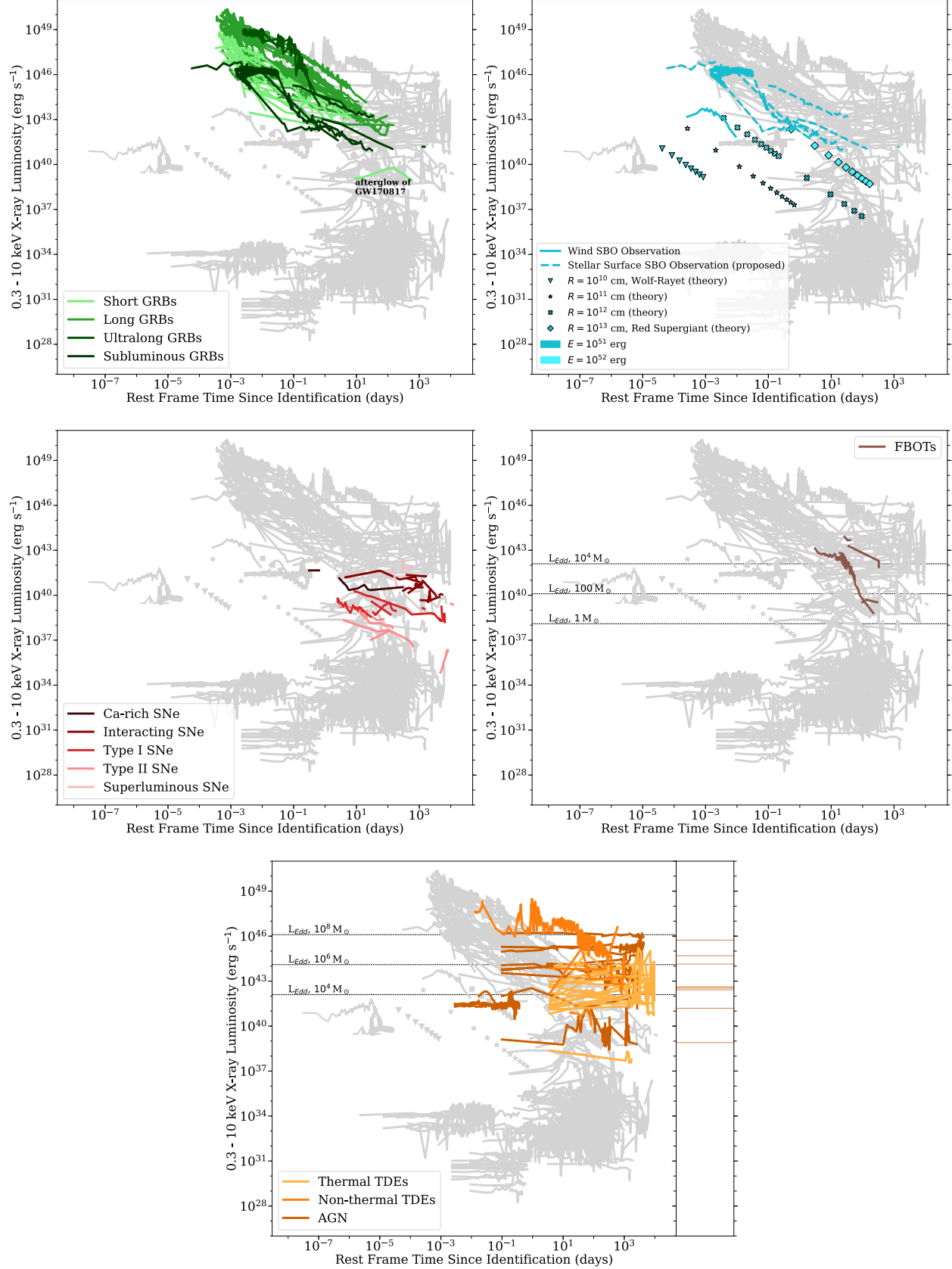
Figure 3. X-ray phase space of extragalactic transients, including GRBs, SBOs, SNe, TDEs, AGN, and FBOTs. We underplot Eddington luminosities (as horizontal dashed lines) for some potentially relevant BH progenitor masses for both FBOTs and TDEs/AGN. The FBOT X-ray counterparts occupy a luminosity range that is intermediate between normal SNe (shades of red) and GRBs (shades of green). At right in the TDE/AGN subplot, we show quiescent AGN luminosities. Included events are listed in Tables A1 through A5.

rial is accreted, resulting in high energy electromagnetic emission from that accretion (Carter & Luminet 1982, 1983).

We include both TDEs with thermal X-ray emission and non-thermal X-ray emission in Figure 3, using Komossa (2015) and Auchettl et al. (2017) to inform our selection of ($z \leq 1$) TDE candidates, showing only *X-ray TDEs* and "*Likely X-ray TDEs*" from the latter. TDEs with non-thermal X-ray emission (from hereon, non-thermal TDEs) belong to a subset of $\sim 10\%$ the TDE population that showed evidence for highly collimated ejecta in the form of relativistic jets (Alexander et al. 2020). There is no evidence for collimation of the thermal X-ray emission which implies that TDEs with thermal X-rays (from hereon, thermal TDEs) are easier to detect. Because there might be similarities between the flare mechanisms of TDEs and active galactic nuclei (AGN) and the distinction between the two classes can be observationally challenging, we opt to show them both in the bottom panel of Figure 3. In the interest of examining only flaring/outbursting behavior, we include long-term variability from AGN, while we exclude changing-look AGN (AGN showing strong spectral variation attendant to changes in flux on very short timescales), which exhibit more persistent variability. We convert the sample of light curves (Auchettl et al. 2018) to our 0.3-10 keV energy band, assuming $\Gamma = 1.8$ (Tozzi et al. 2006). We note that, though we are far from showing *all* AGN light curves in this energy band, we aim to show a representative sample which demonstrates the difficulty in separating TDEs and AGN from light curves alone (for additional AGN/blazar light curves, see e.g., Giommi et al. 2019).

The Quasi-Periodic Eruptions (QPEs) from GSN 069 (Miniutti et al. 2019) occupy a slightly different (similar luminosity, shorter duration) part of the phase space. The physical mechanism that drives QPEs is not fully understood, so we include an example for consistency in looking at AGN outbursting activity, though they may be associated with the same mechanism as changing-look AGN.

While the archetypal non-thermal TDE Swift 1644+57 was initially mistaken for a long GRB, Figure 3 shows that TDEs are clearly distinguished from GRBs for their luminous *and persistent* X-ray emission lasting hundreds of days.

2.5. *Fast Blue Optical Transients*

Fast Blue Optical Transients (FBOTs) are a new class of transient astronomical event, only recently recognized in observations and the literature (e.g., Drout et al. 2014; Arcavi et al. 2016; Tanaka et al. 2016; Pursiainen et al.

2018; Ho et al. 2021). In the optical bands these transients are characterized by short rise times (evolution on the timescale of days) and high luminosities ($L \gtrsim 10^{44}$ erg s^{-1}). We include the five known X-ray instances of this class – CSS161010 (Coppejans et al. 2020), AT2018cow (Rivera Sandoval et al. 2018; Margutti et al. 2019; Rivera Sandoval et al. 2019), AT2020xnd (Bright et al. 2022; Ho et al. 2022), AT2020mrf (Yao et al. 2022), and AT2022tsd (Schulze et al. 2022; Matthews et al. 2022) – in our phase space plot, Figure 3. Until now, only the most luminous optical FBOTs have exhibited detectable X-ray counterparts.

2.6. *Cataclysmic Variables*

Cataclysmic Variables (CVs) are binary systems undergoing mass transfer in which a white dwarf accretes material from a low-mass main sequence companion. The conditions of that mass transfer define the characteristics of the CV outburst. Here we look exclusively at the two classes of CVs that exhibit bursting behavior[4] – (classical and recurrent) novae and dwarf novae.

A nova outburst occurs when the accreted material causes thermonuclear runaway on the surface of the white dwarf, resulting in highly energetic ejection of material from the stellar surface. All X-ray data of novae are from Mukai et al. (2008) and Page et al. (2020). In the instances where we have both an upper- and lower-limit luminosity for various novae in the Mukai sample, we utilized both, to return a *lower-* and *upper*-limit light curve, offering us a greater sense of where novae can, and do, exist in the X-ray phase space (Figure 4). Where k-corrections are necessary to shift data into the (observer frame) 0.3-10 keV band, we adopt a thermal bremsstrahlung spectral model with $kT = 5$ keV following Mukai et al. (2008).

The X-ray emission in dwarf novae stems from the inner accretion flow region around the white dwarf. During the outburst, the mass transfer rate through this inner region increases. As a result it is expected that the X-ray emission (≥ 2 keV) will briefly increase, but then be suppressed as the optical depth of this region increases. This behavior can be seen in multi-wavelength light curves of the dwarf nova SS Cygni (e.g., Wheatley et al. 2003; Russell et al. 2016). Note that there are a number of unanswered questions about this model (see Mukai 2017), and no other dwarf novae show this exact behavior (e.g., Fertig et al. 2011; Mukai 2017). As we are interested in the DLPS of systems that show X-ray

---

[4] We do not include light curves from non-outbursting CVs, like polars, which exhibit low amplitude flickering and flaring due to their stronger magnetic fields (e.g., Angelini & Verbunt 1989).
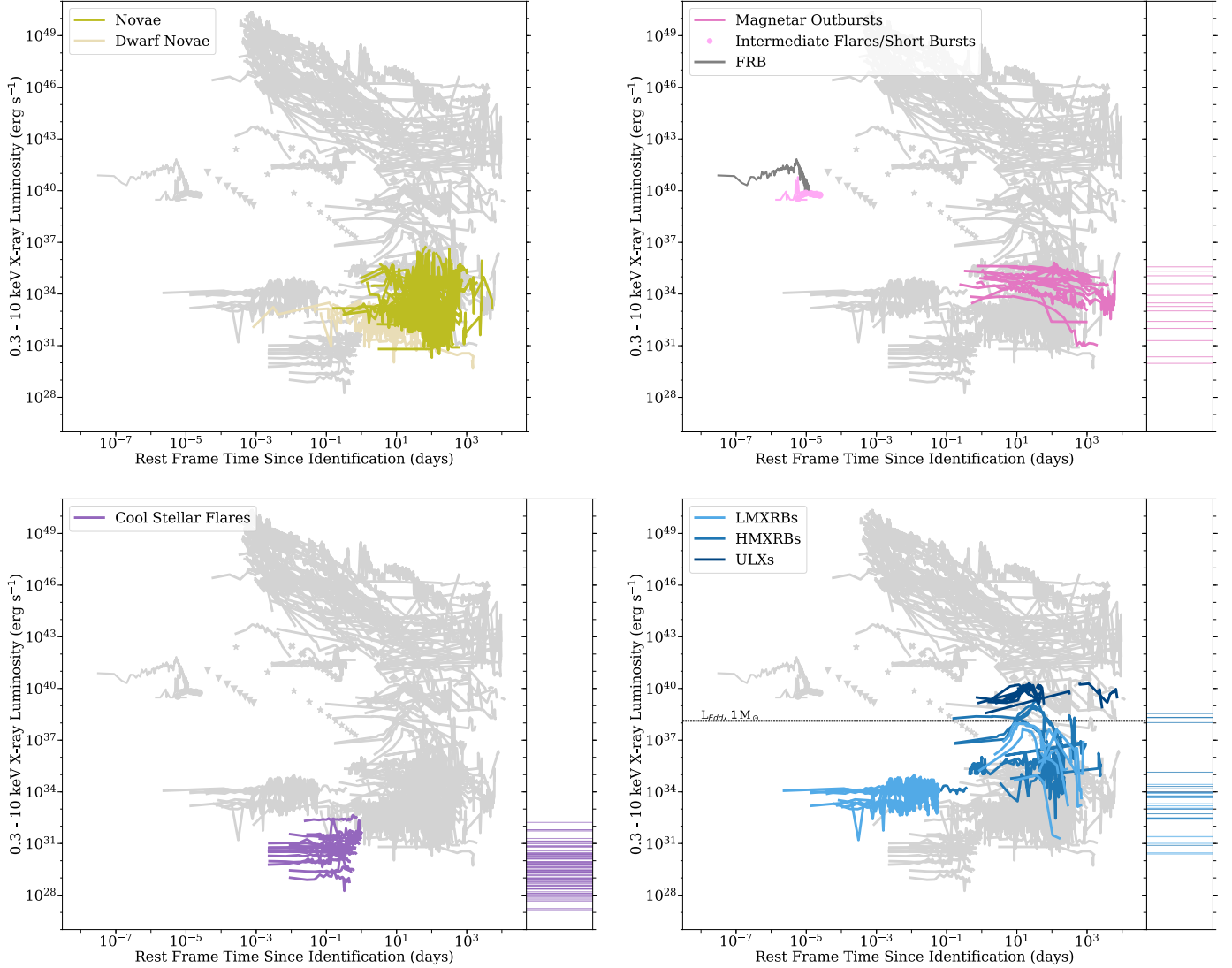
Figure 4. X-ray phase space of Galactic transients and variables, including CVs (novae and dwarf novae), magnetar flares and outbursts, fast radio bursts (specifically the Galactic FRB200428), cool stellar flares, XRBs, and ULXs. We underplot the Eddington luminosity for a $1\,M_\odot$ progenitor for additional context in the XRBs/ULX panel. With the exception of the CV subplot, at right, we show quiescent luminosities for each class of object. Included events are listed in Tables A6 through A9.

brightenings, we limit our sample to those dwarf novae that show X-ray brightenings during optical outburst (see Table A6).

CV outbursts are fairly low luminosity in the $L_x \sim 10^{28} - 10^{36}$ erg s^{-1} range. They are also relatively persistent, evolving over timescales ranging from seconds to years.

2.7. *Magnetar Flares/Outbursts and Fast Radio Bursts*

Magnetar flares/outbursts, driven by perturbations in the strong magnetic field of the magnetar, come in three broad flavors: giant flares (to now, only observed in the hard X-rays and gamma rays), outbursts (characterized by a decay on the scale of days), and intermediate

flares/short bursts (lasting milliseconds to tens of seconds). At gamma-ray energies, the three observed giant flares started with a short (0.1–0.2 s) flash with luminosity from $\approx 10^{44}$ to 10^{46} erg s^{-1}, which was followed by a tail lasting a few hundreds of seconds and modulated at the pulsar spin period. In all three events, the total energy of the tail was $\approx 10^{44}$ erg (e.g. Esposito et al. 2021). While it is likely that a comparable amount of energy was emitted in the soft X-ray band (see Rea et al. 2013), we lack reliable measurements of their properties in that band.

Though intermediate flares and short bursts are often referred to separately, Israel et al. (2008) suggest that these events actually occur along a continuum of spec-

tral properties (though not a continuum in duration or fluence). Making an arbitrary cut, where intermediate flares persist longer and are brighter while short bursts are lower energy and shorter duration, is not based on intrinsically different physics. For the purposes of simplicity in our sub-classifications, we consider intermediate flares and short bursts to be a single population.

We used the Magnetar Outburst Online Catalog (Coti Zelati et al. 2018) for most of the *outburst* data, also including data from Rea et al. (2016) and Esposito et al. (2019) in order to build a *representative* sample. Plotting each light curve from the beginning of the outburst itself, we show each recurrent event from the same progenitor separately. Intermediate flare/short burst data are from Israel et al. (2008).

In order to elucidate the variable nature of these magnetars, we compare their luminosity in outburst (or during a flare) to their quiescent luminosity; we retrieve these data from Olausen & Kaspi (2014)[5] in the 2-10 keV band. We employ a k-correction, assuming a multiple component spectrum ($\Gamma \sim 2$, $kT_{low} \sim 0.3$ keV, $kT_{high} \sim 0.6$ keV) in quiescence (Mong & Ng 2018), to appropriately relate these luminosities to the 0.3-10 keV behavior we have emphasized throughout the X-ray phase space plot. Further, to ensure a one-to-one comparison of the emission from quiescent magnetars and those actively exhibiting variable behavior, we restrict our quiescent L_x sample to match the magnetars shown in the X-ray phase space plot (Figure 4).

Due to the extremely fleeting nature of the short bursts and intermediate flares, much of the data comes from serendipitous triggers, many of which occur in the harder X-rays, since the current class of wide-field instruments operate in the hard X-rays/gamma-rays. This accounts, in part (or in whole), for the paucity of observations for these phenomena in the soft X-rays (and so in our phase space plot) relative to the frequency with which they occur. Where we are dealing with light curves (rather than peak magnitude-duration *points* as with short bursts and intermediate flares) that contain multiple flares/bursts, we reset each successive event to some reasonable offset from $t = 0$ to better populate the X-ray phase space as though by individual signals, taking quiescence to be the lowest observed luminosity between active outburst/flare states.

Fast Radio Bursts (FRBs) are extremely short duration transient events characterized by an intense burst of radio emission (Lorimer et al. 2007; or see Petroff et al. 2019 and Petroff et al. 2022 for reviews). Multiwave-

length follow-up has been conducted to detect counterparts in other wavelength regimes, but efforts have been largely unsuccessful (e.g., Chen et al. 2020). Recently, though, the SGR 1935+2154 outburst on 2020 April 28 has been the subject of discussion as a candidate for an X-ray counterpart to FRB 200428 (The CHIME/FRB Collaboration et al. 2020; Bochenek et al. 2020). Concurrent radio and X-ray emission from this source was detected again in October 2022 (Dong & CHIME/FRB Collaboration 2022; Wang et al. 2022).

Because there is evidence linking this event to a magnetar progenitor, we include the FRB light curve (Li et al. 2021) in Figure 4. The coincident X-ray event from SGR 1935+2154 is consistent with the apparent continuum behavior of magnetar outbursts, flares, and bursts across the phase space and is indicative of the possibility that some FRBs might be the radio counterparts to soft gamma repeaters (see however Pleunis et al. 2021).

2.8. *Cool Stellar Flares*

Cool, low mass stars, such as M-dwarfs, can be highly variable, with energetic flares driven by magnetic reconnection events. The intensity of this behavior is also correlated with age, with younger low-mass stars exhibiting more variability.

We place data from Pye et al. (2015) in Figure 4 and assume a thermal spectral model with a temperature of $kT = 1.5$ keV in order to perform the flux conversion. Dwarf stars included in our sample are K, M, and L types. As in Section 2.7, quiescent luminosities (digitized from Pye et al. 2015) are plotted at the right to appropriately contextualize the flares and offer yet more indication of where these flaring stars exist in the X-ray phase space. Cool stellar flares are relatively short duration, with timescales ranging from on the order of hundreds of seconds up to ~ 1 day. They are also low luminosity[6] events with $L_x \gtrsim 10^{28}$ erg s^{-1} and up to several $\times 10^{32}$ erg s^{-1}. Quiescent luminosities span the range $\sim 10^{27} - 10^{32}$ erg s^{-1}.

2.9. *X-ray Binary Outbursts and Ultraluminous X-ray Sources*

X-ray binaries (XRBs) are stellar binaries where a compact object (neutron star or black hole) is accreting material from its companion, causing energetic outbursts. Ultraluminous X-ray sources (ULXs, characterized by peak $L_x > 10^{39}$ erg s^{-1}, independent of the

---

[5] http://www.physics.mcgill.ca/~pulsar/magnetar/main.html

[6] We note that all sky survey data has shown intrinsically rare flares up to $L_x \sim 10^{34}$ at slightly higher energies (2 - 20 keV) (Tsuboi et al. 2016).

source's underlying mechanism) are frequently associated with super-Eddington XRBs. We also elect to group them here, showing them in the same subplot of Figure 4. XRBs are further broken out into high mass (HMXRBs, with a primary star of mass ≥ 10 M$_\odot$; for a review, see Reig 2011) and low mass (LMXRBs, with a $1 \leq M/M_\odot < 10$ primary; for a review, see Tetarenko et al. 2016) populations. The former includes BeXRBs, supergiant X-ray binaries (SGXRBs), and supergiant fast X-ray transients (SFXTs), while the latter includes neutron star X-ray binaries (NS-XRBs) and black hole X-ray binaries (BH-XRBs). Details of the relevant data and their provenance are in Table A9.

As with the other variable signals (magnetar outbursts and M-dwarf flares, top right and bottom left of Figure 4), we plot the quiescent L$_x$ of ULX and XRB events at the right in Figure 4. As in Section 2.7, for the purposes of this paper, we define the quiescent luminosity as the lowest recorded X-ray luminosity, opting for simplicity rather than a more stringent definition that might not designate this persistent, non-outburst behavior as quiescence. Though we are not aiming for completeness, choosing instead to use a *representative* sample, the XRB and ULX coverage of the phase space is clear for relatively long timescales ranging from tenths to thousands of days and intermediate luminosities. XRBs exist in roughly the $L_x \sim 10^{32}-10^{39}$ erg s^{-1} range (with quiescent luminosities between 10^{30} and 10^{35} erg s^{-1}). ULXs have luminosities greater than several $\times 10^{38}$ erg s^{-1} and up to $\sim 10^{40}$ erg s^{-1}, with quiescent L$_x$ falling between 10^{38} and 10^{39} erg s^{-1}.

In regards to target selection, it is necessary to use a sample of sources with well measured distances. We note that many of the Galactic HMXRBs have poorly measured distances with high uncertainties (e.g. Bartlett et al. 2019; Ferrigno et al. 2022), while their soft X-ray spectra might suffer from strong absorption. However, nearby galaxies of the Small and Large Magellanic Clouds (i.e. SMC and LMC) have well defined distances, low foreground absorption and an abundance of HMXRBs (Haberl & Sturm 2016). Thus a representative sample of HMXRB outbursts can be obtained from the SMC and LMC.

3. DISCUSSION

3.1. *Unclassified X-ray Sources: A Short Case Study*

With the rise of time-domain astronomy, there has been a commensurate increase in opportunities to capture new types of transient/variable events that defy all known classification schemes. In some cases, these events have been discovered in archival data searches, thus preventing real time follow-up of these events out-

side the X-rays. This has practically prevented the identification of the true underlying nature of these new classes of events. In Figure 5, we plot a selection of these yet-unidentified "oddballs" (Jonker et al. 2013; Glennie et al. 2015; Bauer et al. 2017; Novara et al. 2020) to illustrate how they fit into the larger X-ray phase space. We include only those with known or estimated distances (assuming for the purposes of this case study that the X-ray phase space of transients for $z \leq 1$ is similar to the phase space of transients at all redshifts), and spectra for those observed outside of the 0.3 - 10 keV band to facilitate a k-correction.

Where multiple distance estimates are given, we include light curves at each of those distances to better fill out the *uncategorized* X-ray phase space and demonstrate the potentially varied interpretations of these signals at different redshifts. Though they are sometimes referred to as fast X-ray transients (FXTs or FXRTs, see e.g. Quirola-Vásquez et al. 2022 for a population-level examination), the light curves point to these transients having a variety of progenitors. This inhomogeneous class of transient events evolves on timescales of ~ 10s of seconds to days and spans roughly 21 dex in luminosity.

Where the discovery papers have broadly speculated about the origin of these transients, we have colored the "oddball" light curves accordingly, allowing their position in the DLPS to discriminate between equally likely physical scenarios. In fact, this is an extension of the analysis done in Bauer et al. (2017), where they illustrate potential classifications by comparing CDF-S XT1 to light curves from already classified events. Where no one potential class is favored in the discovery paper we choose to leave the light curve *uncategorized* in the X-ray phase space (CDF-S XT1), whereas we color those with a single (or preferred) proposed origin according to that theory (XRT 000519, XRT 120830, and XRT 110103, EXMM 023135.0-603743). Jonker et al. (2013) prefers the (beamed) tidal disruption of a white dwarf by an intermediate mass black hole for XRT 000519, though our results suggest that an X-ray flash (as would be associated with a GRB) would also be reasonable. Taking XRT 000519 as potentially related to XRT 110103, Glennie et al. (2015) suggest the same potential progenitors for that event. They also indicate that XRT 120830 seems consistent with a dwarf star flare, which is borne out by its position in the phase space. Similarly, Novara et al. (2020) posit that EXMM 023135.0-603743 could be a shock breakout from a core-collapse supernova, a possibility which is supported by the light curve's position in the phase space, while also noting that it could be an AGN, a TDE, or even a late-time observation of
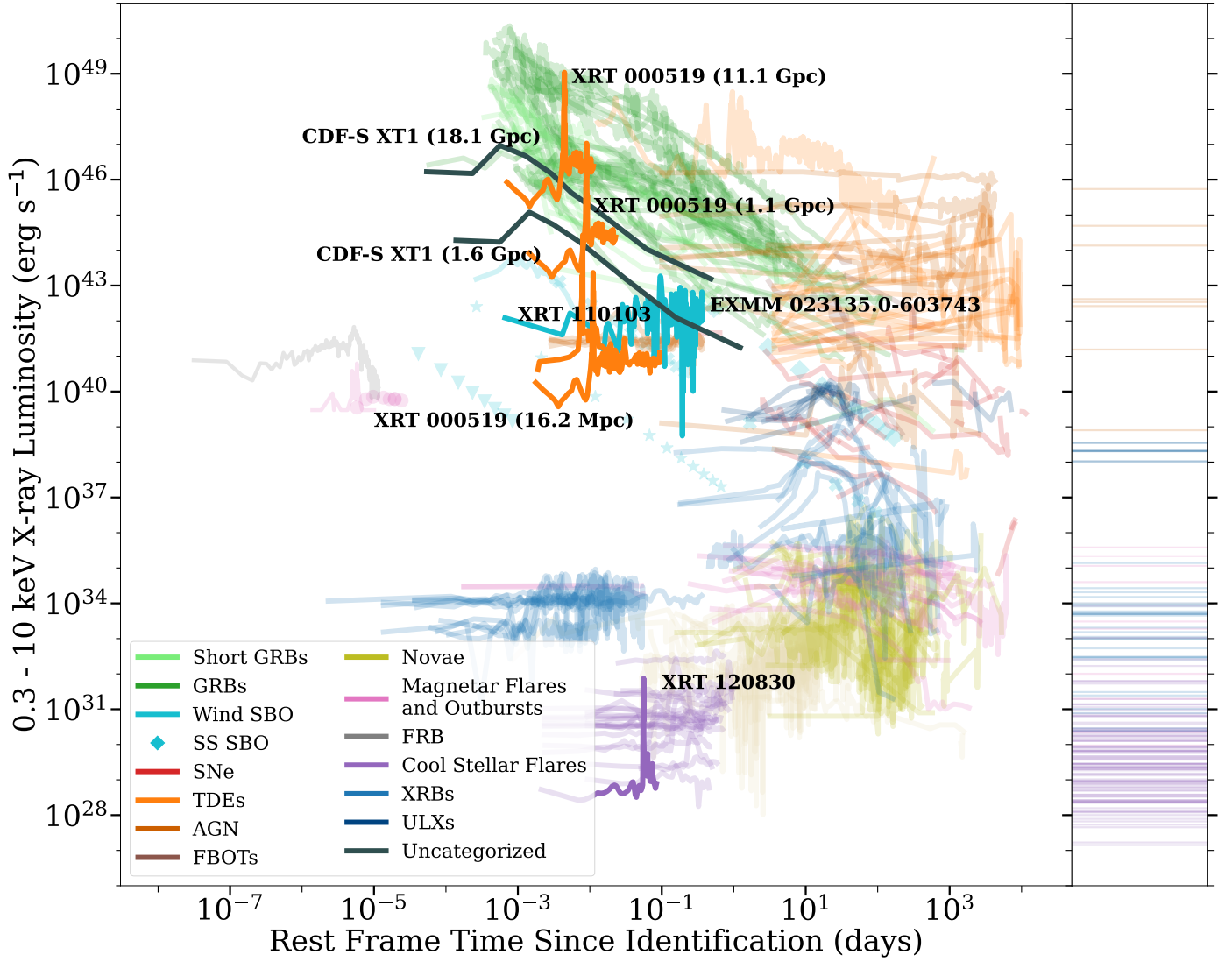
Figure 5. We compare existing observations of transients with unclear/debated classification with our established X-ray phase space as described in Section 3.1. These signals are colored according to their preferred classification, though in cases where no one model is considered a better match (CDF-S XT1), we give them their own "oddball" color to differentiate them from the already classified transients in the phase space. For sources with uncertain distance estimates, each estimate is shown, with the relevant distance stated in parentheses. Included events are listed in Table A10.

a giant flare from a magnetar, though each of those scenarios is disfavored given other concurrent data (Novara et al. 2020).

Ultimately it is clear that, while the DLPS is not able to provide classification for transients/variables without input from the signal's spectral evolution and from other investigations that hint at the underlying mechanism, it is extremely useful to contextualize potential and preliminary classifications. As we see looking at the 16.2 Mpc XRT 000519 light curve and XRT 110103, their position in the phase space is apparently more consistent with an AGN/QPE than with a TDE, the potential confusion in classification stemming from the innate difficulty in distinguishing TDEs and AGN. For

greater distances, the light curve characteristics of XRT 000519 seem to potentially align with a GRB-related X-ray flare. Similarly, while CDF-S XT1 has a myriad of potential progenitors (among them, an off-axis short GRB or a subluminous GRB, another white dwarf-intermediate mass black hole TDE; Bauer et al. 2017), the light curve (assuming a distance of 18.1 Gpc) is nicely consistent with the subluminous GRBs in our sample.

3.2. *Discovery Space*

As we enter a new era in the search for/detection of X-ray transients and variables, due to both large time-domain surveys and next generation X-ray observato-

ries, it is crucial to understand the observational restrictions that have inherently shaped our understanding of the high energy transient sky to now. In examining the phase space of existing detections, we find that while both the most luminous (largely extragalactic) and least luminous (largely Galactic) part of the phase space is well-populated at $t > 0.1$ days, intermediate luminosity phenomena ($L_x = 10^{34} - 10^{42}$ erg s^{-1}) represent a gap in the phase space. We thus identify $L_x = 10^{34} - 10^{42}$ erg s^{-1} and $t = 10^{-4} - 0.1$ days as a key discovery phase space in transient X-ray astronomy (see Figure 6).

The most obvious constraints are the sensitivity limits of current instruments and the difficulty of rapid response to a fleeting and intrinsically rare signal, which leave gaps in our phase space at low luminosities and short durations respectively. Due to inherent design constraints (see Figure 7, discussed more in Section 3.3) current instruments generally fall into one of two categories – instruments that are likely to contribute to the serendipitous discovery of soft X-ray transients, which have limited sensitivity and instruments that allow for follow up of event evolution down to very deep limits, which are extremely limited in their field of view..

Instruments with a wide field of view will serendipitously detect many more events than targeted instruments, contributing to the discovery of transient signals alongside survey instruments. Realistically, extremely short-duration events (on the order of seconds) will not be observed with any regularity without a new generation of wide field instruments. This regime of extremely rapid events is already known to include FRB X-ray counterparts and their likely relatives, magnetar flares.

Target of Opportunity (ToO) protocols and other similar observational triggers play a role in successful follow up of transitory signals. Greater efficiency in the form of fast re-pointings will also help push toward observation of extremely short-duration events; for instance, the robust *Swift* ToO process is well-established. Automated follow-up is not restricted to the X-ray with high-energy transient detections triggering radio observations (e.g. Staley et al. 2013; Hancock et al. 2019), as well.

Projects such as Exploring the X-ray Transient and variable Sky (EXTraS; De Luca et al. 2021) aim to address the gap in the short duration phase space at the algorithmic level, extracting previously unidentified signals and variability from existing XMM-Newton data (e.g., Novara et al. 2020).

Efforts to rapidly disseminate information about detections like the Living *Swift*-XRT Point Source catalog (Evans et al. 2022) offer yet-other opportunities for expedient analysis and follow-up.

More sensitive instruments are key for targeted follow-up. The next generation of highly sensitive soft X-ray missions will enable us to track the evolution of light curves to much later times/lower luminosities as they decay and will provide a broader understanding of transient populations, as in many cases, we are currently only meaningfully sampling the most luminous end of the population.

Figure 6 also reveals an under-sampled area of the phase space that we should aim to explore. On the interval $L_x = 10^{34} - 10^{42}$ erg s^{-1} and with timescales between 10^{-4} and ~ 0.1 days, there is a clear gap in the phase space. This gap also corresponds to some known physical phenomena – stellar surface shock breakouts (see Section 2.2) and the continuum behavior between magnetar flares and outbursts (see Section 2.7). Efforts to expand observations in this regime should be motivated by the probable detection of these missing signals.

3.3. *Rates of transient discovery*

There is a well-known trade-off between instrument FOV and sensitivity, as shown in Figure 7, using specifications from currently operating and proposed missions: larger FOVs tend to correlate with lower sensitivities.

Making the reasonable assumption that we have already observed the most luminous events from each sub-class of transient/variable, we can decouple the advantages of increased FOV and increased sensitivity with transient peak luminosities and volumetric rates from Stone & Metzger (2016), Coppejans et al. (2020), Margutti & Chornock (2021), and Ghirlanda & Salvaterra (2022), separately examining the importance of wide-field instruments and extremely sensitive instruments. For the GRBs (both long and short), we apply a beaming correction factor based on a conservative jet opening angle of $\sim 3°$ (Fong et al. 2015; Rouco Escorial et al. 2022). We can isolate the impact of increased FOV by effectively marginalizing over sensitivity and looking at the number of observations as a function of field of view. We choose a representative sensitivity of 10^{-13} erg s^{-1} cm^{-2} and assume a static pointing, so that the importance of signals serendipitously falling in that FOV is clear. We show this plot on the left side of Figure 8. Similarly, we can look at the importance of increased sensitivity by selecting a representative FOV (1 deg^2) and plotting the number of observations per class of transient as a function of sensitivity. This is shown on the right side of Figure 8. As in the rest of the paper, we limit our events and observing depths to the redshift range in which their rates are well-constrained ($z \leq 1$).

We can also use this maximum luminosity along with the instrument sensitivity to determine the distance out
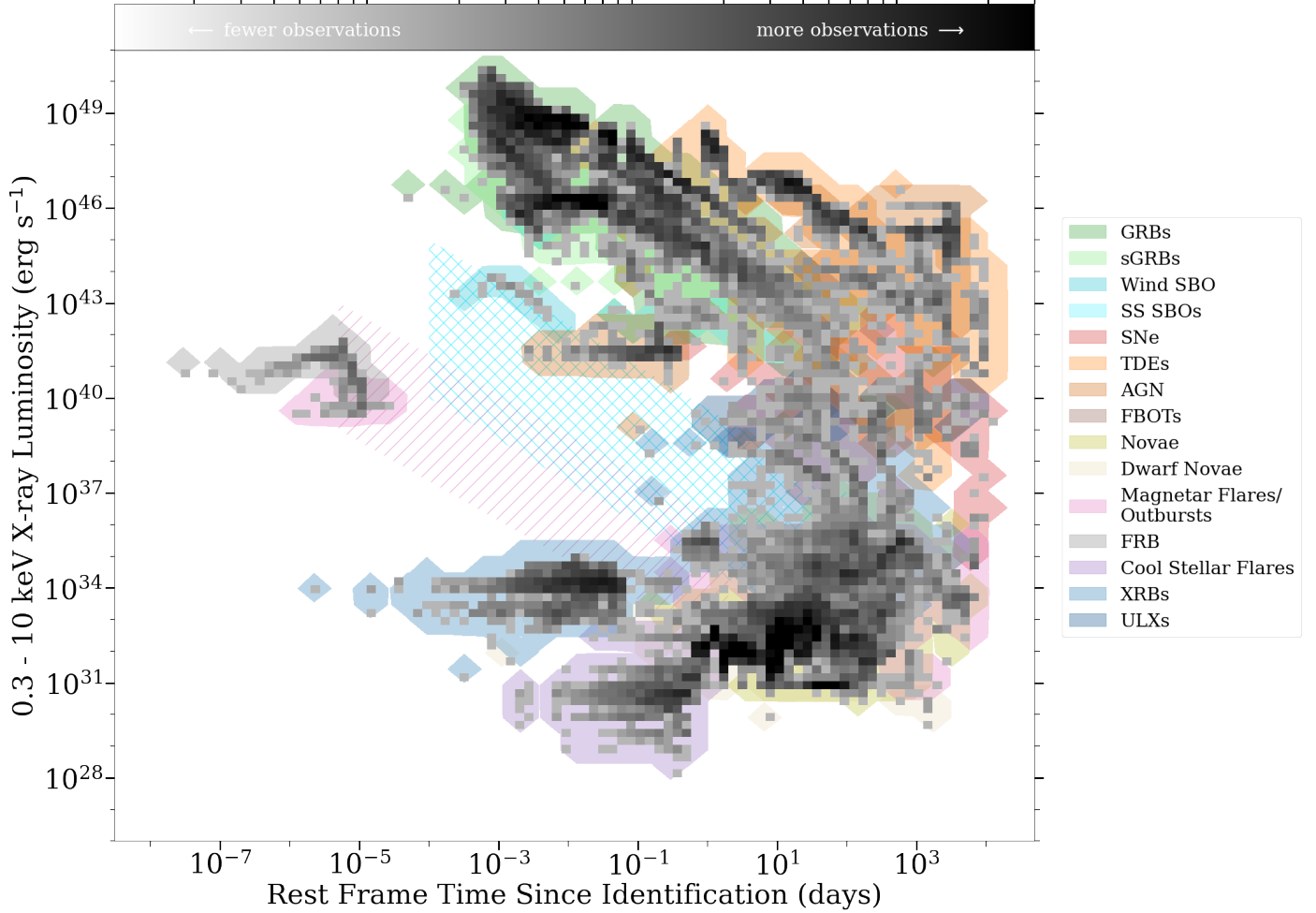
Figure 6. The density of light curves in our phase space with the corresponding classes of transient underplotted; the colorbar is logarithmic and larger bins were used for the transient classes than for the overall observations. Though we only show the density of data included in this paper (and so not the comprehensive density of *all* observations in this energy band), certain trends are notable that are generally relevant, including that the best sampled classes of transient are either Galactic phenomena (such as cool stellar flares or novae) or high luminosity extragalactic transients such as GRBs and short GRBs and that there is a paucity of observations of relatively short duration events at intermediate luminosities. We use hatches to mark the general region of the phase space where we would anticipate, but do not yet have, observations of magnetar flares and outbursts (pink) and shock breakouts from stellar explosions (light blue) among other events.

to which each transient/variable event can be observed. We take the maximum luminosity of the transient in the GRB, SBO, SN, TDE, CV, magnetar flare/outburst, M-dwarf flare, XRB, ULX, FBOT, and FRB categories to represent the most luminous end of their respective distributions. We then apply the 0.3-10 keV flux limit (as in Figure 7 and Table 1) to determine the luminosity distance out to which the transient can be detected, from which we estimate the comoving distance.

For Galactic transients, we show the luminosity distance out to which various transients can be observed vs. the fraction of the sky covered instantaneously by the instrument FOV in Figure 9. As in the rest of this work, we limit instrument depth to a maximum luminosity distance that corresponds to $z = 1$. Needless

to say, the qualitative trends captured by our Galactic transient observing volume plot (Figure 9) translate to the behavior of extragalactic sources, with targeted instruments being more conducive to observing distant phenomena, while wide-field instruments have considerably shallower sky coverage.

For extragalactic transients, we instead examine an estimate of the number of observed events per year for each class of phenomena broken down by instrument. Using the three-dimensional observing volumes, defined as $\frac{\text{FOV}}{\Omega} \times \frac{4}{3}\pi\, d_{\text{com}}^3$, and the same volumetric rates as in Figure 8, we construct Figure 10.

4. CONCLUSION

Table 1. Soft X-ray imaging instrument performance parameters. We use the horizontal bars to differentiate between three categories of instrument, from top to bottom we list past instruments, currently operational instruments, instruments on future missions selected for launch, and instruments on proposed missions. The list of proposed missions is not complete and it is provided to illustrate the range of capabilities of future experiments.

Instrument	Energy band (keV)	Flux limit[a] (erg s^{-1} cm^{-2})	FOV	References
ROSAT/PSPC-C	0.1 - 2.5	$\sim 10^{-13}$	$3\,\mathrm{deg}^2$	Briel et al. 1996
				Greiner et al. 1999
Chandra ACIS-S[b]	0.5 - 7	$\sim 3 \times 10^{-14}$	$16.'9 \times 16.'9$	Chandra X-ray Center et al. 2021
Swift/XRT	0.3 - 10	$\sim 2 \times 10^{-13}$	$23.'6 \times 23.'6$	Burrows et al. 2005
				Evans et al. 2020
MAXI GSC	2 - 30	$\sim 9 \times 10^{-11}$	$160° \times 3°$	Sugizaki 2010
MAXI SSC	0.5 - 12	$\sim 2 \times 10^{-10}$	$90° \times 1.°5$	Tsunemi et al. 2010
XMM-Newton/EPIC-pn	0.2 - 10	$\sim 3 \times 10^{-14}$	$27.'5 \times 27.'5$	Watson et al. 2001
SRG/eROSITA	0.2 - 8	$\sim 10^{-13}$	$0.8\,\mathrm{deg}^2$	Merloni et al. 2012
NICER	0.2 - 12	$\sim 8 \times 10^{-14}$	$30\,\mathrm{arcmin}^2$	Arzoumanian et al. 2014
Insight-HXMT/LE	0.9 - 12	$\sim 1.5 \times 10^{-11}$	$21\times(1.°6\times6°), 7\times(4°\times6°),$	Li et al. 2020b
			$2\times(50\sim60°\times2\sim6°)$	
			or $\sim 810\,\mathrm{deg}^2$ total	
SVOM/MXT	0.2 - 10	$\sim 4 \times 10^{-12}$	$64' \times 64'$	Wei et al. 2016
XRISM/Xtend[c]	0.4 - 13	$\sim 6 \times 10^{-14}$	$38' \times 38'$	XRISM Team,
				Private Communication
Athena/WFI	0.2 - 15	$\sim 5 \times 10^{-16}$	$40' \times 40'$	Barcons et al. 2012
eXTP/WFM	2 - 50	$\sim 9 \times 10^{-11}$	$\sim 180° \times 90°$	Zhang et al. 2019
AXIS	0.1 - 10	$\sim 2 \times 10^{-16}$	$144\pi\,\mathrm{arcmin}^2$	Mushotzky 2018
Einstein Probe/WXT	0.5 - 4	$\sim 2 \times 10^{-11}$	$3600\,\mathrm{deg}^2$	Yuan 2017
STAR-X	0.5 - 6	$\sim 3 \times 10^{-14}$	$1\,\mathrm{deg}^2$	STAR-X Team,
				Private Communication
STROBE-X	0.2 - 12	$\sim 5 \times 10^{-14}$	$4\pi\,\mathrm{arcmin}^2$	Ray et al. 2019
				Meidinger 2018
Lynx/HDXI	0.2 - 10	$\sim 1.5 \times 10^{-18}$	$22' \times 22'$	The Lynx Team 2019
THESEUS/SXI	0.3 - 5	$\sim 2 \times 10^{-11}$	$\sim 0.5\,\mathrm{sr}$	Amati et al. 2021

[a] 0.3-10 keV; all flux limits are k-corrected to our band-of-interest assuming a fiducial $\Gamma = 2$ spectrum. Flux limit is based on a 1 ks exposure for instruments that do pointed observations. We note that for instruments designed for higher energy observations – such as MAXI GSC or eXTP/WFM – our estimated flux limit in the 0.3 - 10 keV band is less secure.

[b] The reported Chandra 0.3 - 10 keV flux limit is estimated from recent observations

[c] We take the full-band Suzaku/XIS flux limit from Miura et al. (2008), given its sensitivity is roughly comparable to that of XRISM/Xtend (XRISM Team, Private Communication).

With the immense promise of next generation X-ray instruments on the horizon and community investment in large time-domain surveys, many more X-ray transients will be detected and studied in the coming years. We construct a set of observational X-ray phase space plots, which show distinctions between different transient and variable phenomena and highlight the luminosity evolution of these events using real light curves. The X-ray duration-luminosity phase space can be used to help disambiguate the nature of newly observed signals by placing them in context (even before spectroscopic or multi-wavelength follow-up, as demonstrated in Section 3.1) and to point out sparse areas of the phase space that should be the focus of future exploration.

As expected, the phase space is less populated at extremely low luminosities and extremely short durations, given the limitations of current instruments and the trade-off between FOV and sensitivity in instrument design. More sensitive imagers will provide better insight into less luminous events, but wide-field imagers will be

Table 2. Estimated rate (in yr^{-1}) of serendipitous detections of extragalactic transients in a single pointing of each soft X-ray instrument.

Instrument	sGRBs	lGRBs	SNe	SLSNe	non-thermal TDEs	thermal TDEs	SBOs	FBOTs
ROSAT	6.28×10^{-3} 8.98×10^{-11}	$5.34 10^{-3}$ $8.31 10^{-8}$	0.140 9.40×10^{-12}	4.29×10^{-3} 1.05×10^{-5}	1.15×10^{-4} 9.81×10^{-8}	1.15×10^{-2} 1.59×10^{-12}	7.74 2.85×10^{-2}	0.494 3.62×10^{-8}
Chandra	1.66×10^{-4} 1.25×10^{-11}	1.41×10^{-4} 1.11×10^{-8}	1.80×10^{-2} 1.31×10^{-12}	5.03×10^{-4} 1.42×10^{-6}	3.03×10^{-6} 1.19×10^{-8}	3.03×10^{-4} 2.22×10^{-13}	0.684 3.57×10^{-3}	4.19×10^{-2} 5.04×10^{-9}
Swift/XRT	3.24×10^{-4} 1.64×10^{-12}	2.75×10^{-4} 1.54×10^{-9}	2.66×10^{-3} 1.72×10^{-13}	8.44×10^{-5} 1.93×10^{-7}	5.91×10^{-6} 1.90×10^{-9}	5.69×10^{-4} 2.91×10^{-14}	0.177 5.43×10^{-04}	1.16×10^{-2} 6.62×10^{-10}
MAXI GSC	1.01 5.35×-13	0.854 5.20×10^{-10}	9.43×10^{-4} 5.61×10^{-14}	3.33×10^{-5} 6.45×10^{-8}	1.83×10^{-2} 7.17×10^{-10}	1.18×10^{-3} 9.46×10^{-15}	0.118 1.97×10^{-4}	8.51×10^{-3} 2.16×10^{-10}
MAXI SSC	0.283 4.54×10^{-14}	0.240 4.42×10^{-11}	8.01×10^{-5} 4.75×10^{-15}	2.84×10^{-6} 5.48×10^{-9}	5.16×10^{-3} 6.10×10^{-11}	1.07×10^{-4} 8.03×10^{-16}	1.01×10^{-2} 1.68×10^{-5}	7.36×10^{-4} 1.83×10^{-11}
XMM Newton	4.40×10^{4} 3.81×10^{11}	$3.74 10^{-4}$ $3.38 10^{-8}$	5.43×10^{-2} 4.01×10^{-12}	1.51×10^{-3} 4.33×10^{-6}	8.02×10^{-6} 3.58×10^{-8}	8.02×10^{-4} 6.79×10^{-13}	2.00 1.08×10^{-2}	0.122 1.54×10^{-8}
eRosita	2.09×10^{-3} 2.99×10^{-11}	1.78×10^{-3} 2.77×10^{-11}	4.68×10^{-2} 3.13×10^{-12}	1.43×10^{-3} 3.50×10^{-6}	3.82×10^{-5} 3.27×10^{-8}	3.82×10^{-3} 5.31×10^{-13}	2.58 9.49×10^{-3}	0.165 1.21×10^{-8}
NICER	1.74×10^{-5} 3.48×10^{-13}	1.48×10^{-5} 3.20×10^{-10}	5.38×10^{-4} 3.65×10^{-14}	1.62×10^{-5} 4.05×10^{-8}	3.18×10^{-7} 3.72×10^{-1}	3.18×10^{-5} 6.19×10^{-15}	2.77×10^{-2} 1.09×10^{-4}	1.75×10^{-3} 1.41×10^{-10}
Insight-HXMT/LE	1.70 1.33×10^{-11}	1.44 1.29×10^{-8}	2.32×10^{-2} 1.39×10^{-12}	8.14×10^{-4} 1.60×10^{-6}	3.09×10^{-2} 1.76×10^{-8}	2.31×10^{-2} 2.35×10^{-13}	2.73 4.85×10^{-3}	0.195 5.35×10^{-9}
SVOM/MXT	2.38×10^{-3} 1.35×10^{-13}	2.03×01^{-3} 1.31×01^{-10}	2.34×10^{-4} 1.41×10^{-14}	8.11×10^{-6} 1.62×10^{-8}	4.35×10^{-5} 1.76×10^{-10}	1.73×10^{-4} 2.39×10^{-15}	2.52×10^{-2} 4.89×10^{-5}	1.77×10^{-3} 5.46×10^{-11}
XRISM/Xtend	8.40×10^{-4} 2.58×10^{-11}	7.14×10^{-4} 2.35×10^{-8}	3.90×10^{-2} 2.70×10^{-12}	1.15×10^{-3} 2.99×10^{-6}	1.53×10^{-5} 2.67×10^{-8}	1.53×10^{-3} 4.59×10^{-13}	1.83 7.84×10^{-3}	0.115 1.04×10^{-8}
Athena WFI	9.31×10^{-4} 3.50×10^{-8}	7.91×10^{-4} 1.94×10^{-5}	20.4 3.94×10^{-9}	0.314 2.89×10^{-3}	1.70×10^{-5} 9.24×10^{-6}	1.70×10^{-3} 6.58×10^{-10}	12.0 3.46	0.509 1.42×10^{-5}
eXTP/WFM	33.9 1.80×10^{-11}	28.8 1.76×10^{-8}	3.18×10^{-2} 1.89×10^{-12}	1.12×10^{-3} 2.18×10^{-6}	0.619 2.42×10^{-8}	3.99×10^{-2} 3.19×10^{-13}	3.97 6.66×10^{-3}	0.287 7.28×10^{-9}
AXIS	2.63×10^{-4} 3.75×10^{-8}	2.24×10^{-4} 1.66×10^{-5}	15.0 4.40×10^{-9}	9.60×10^{-2} 2.63×10^{-3}	4.80×10^{-6} 4.80×10^{-6}	4.80×10^{-4} 7.28×10^{-10}	3.38 2.42	0.144 1.53×10^{-5}
Einstein Probe/WXT	7.54 3.83×10^{-11}	6.41 3.72×10^{-8}	6.71×10^{-2} 3.99×10^{-12}	2.36×10^{-3} 4.61×10^{-6}	0.138 5.09×10^{-8}	7.00×10^{-2} 6.77×10^{-13}	7.99 1.40×10^{-2}	0.573 1.54×10^{-8}
STAR-X	2.09×10^{-3} 1.81×10^{-10}	1.78×10^{-3} 1.61×10^{-7}	0.259 1.91×10^{-11}	7.18×10^{-3} 2.06×10^{-5}	3.82×10^{-5} 1.71×10^{-7}	3.82×10^{-3} 3.23×10^{-12}	9.51 5.13×10^{-2}	0.580 7.32×10^{-08}
STROBE-X	7.31×10^{-6} 2.95×10^{-13}	6.21×10^{-6} 2.67×10^{-10}	4.40×10^{-4} 3.09×10^{-14}	1.28×10^{-5} 3.40×10^{-8}	1.33×10^{-7} 2.98×10^{-10}	1.33×10^{-5} 5.24×10^{-15}	1.94×10^{-2} 8.81×10^{-5}	1.21×10^{-3} 1.19×10^{-10}
Lynx/HDXI	2.82×10^{-4} 2.62×10^{-5}	2.39×10^{-4} 2.39×10^{-4}	0.362 7.16×10^{-6}	0.103 0.103	5.14×10^{-6} 5.14×10^{-6}	5.14×10^{-4} 9.33×10^{-7}	3.62 3.62	0.154 1.13×10^{-2}
THESEUS/SXI	6.51 3.31×10^{-11}	5.54 3.21×10^{-8}	5.80×10^{-2} 3.45×10^{-12}	2.04×10^{-3} 3.99×10^{-6}	0.119 4.40×10^{-8}	6.05×10^{-2} 5.85×10^{-13}	6.90 1.21×10^{-2}	0.495 1.33×10^{-8}

Note—For each instrument we show an upper (top) and lower (bottom) limit for the serendipitous observation rate. The upper limit is based on the observing volume calculated for the most luminous observation of an event in that class, while the lower limit is based on the observing volume calculated for the least luminous observation of an event in that class. As in Table 1, we separate past, present, planned, and proposed instruments with horizontal lines.

necessary to serendipitously capture the most ephemeral signals, like those of candidate FRB counterparts. There is another, less intuitive gap in the phase space around $L_x = 10^{34} - 10^{42}$ erg s^{-1} and duration $10^{-4} - 0.1$ days. We expect this part of the X-ray phase space to include both SBOs and magnetar flares. Additional observations targeting this part of the phase space will not only increase the studied population of known classes of transient, but will potentially uncover yet-unidentified signals, as well.

Software: AstroPy (Astropy Collaboration et al. 2013, 2018), Matplotlib (Hunter 2007), NumPy (Harris et al. 2020), pandas (pandas development team 2020; Wes McKinney 2010), PIMMS (Mukai 1993), scikit-learn (Pedregosa et al. 2011), SciPy (Virtanen et al. 2020), WebPlotDigitizer (Rohatgi 2019)
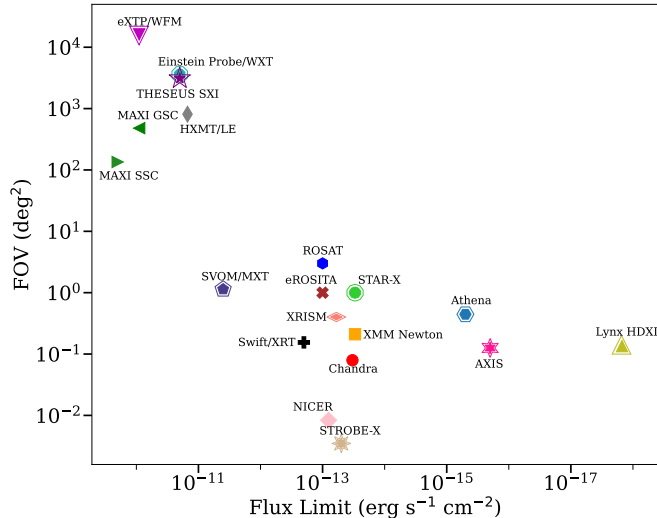
Figure 7. Here we show the roughly inverse relation between instrument FOV and depth with a summary of these specifications for existing and planned/proposed X-ray missions (see Table 1 for more details). We report the 1 ks 0.3-10 keV sensitivity. Upcoming/proposed instruments are highlighted by an additional marker outline.

APPENDIX

A. DATA

We list here all of the events included in the paper. For each event, we also provide coordinates, distance, and references, and, where applicable, we provide sub-classification. For GRBs, we also list redshift and T_{90}. These data are available on GitHub (see Section 2), with a few limited exceptions, which are marked clearly in the tables below. Quoted distances are luminosity distances for the cosmology indicated in Section 1.

B. THE TRUE OBSERVER'S PHASE SPACE: FLUX VS. DURATION

While the luminosity X-ray phase space is very instructive for understanding which physical phenomena are poorly captured by current instruments, it does little to reinforce the role that instrument sensitivity plays in determining which phenomena are detected. We show a purely observational duration-flux phase space in Figure 11.

Future missions will improve substantially on current sensitivity limits. This will open up an innately new area of the low luminosity parameter space, significantly extending the depth out to which known classes of transients can be detected and potentially revealing the existence of yet-unknown intrinsically faint signals.
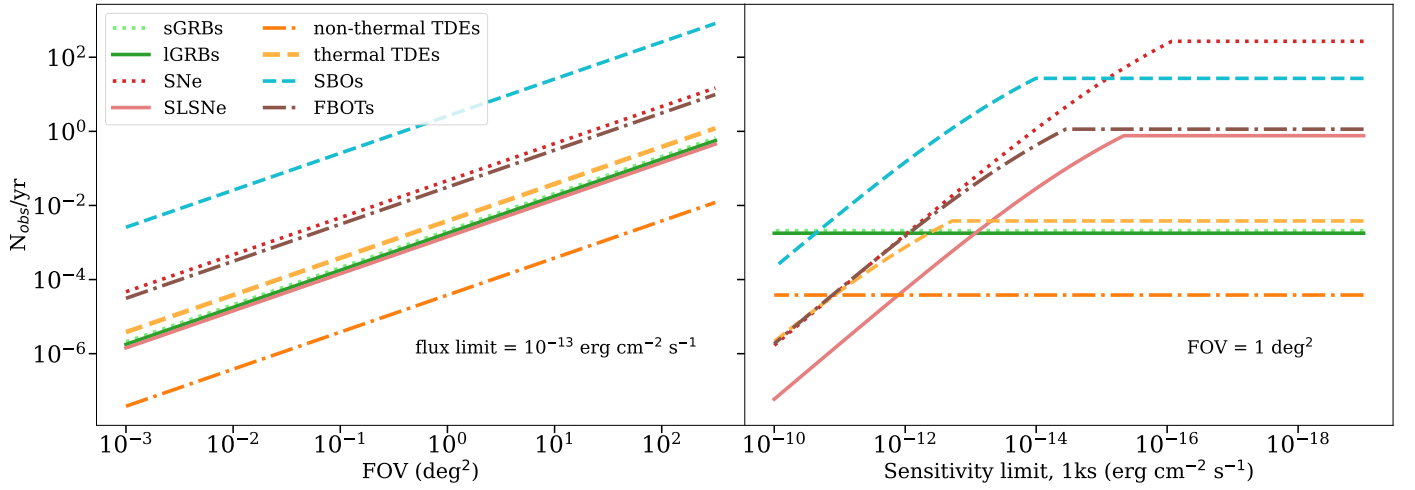
Figure 8. To decouple the advantages of increased field of view and sensitivity, we show extragalactic transient rates (Stone & Metzger 2016; Coppejans et al. 2020; Margutti & Chornock 2021; Ghirlanda & Salvaterra 2022) as a function of FOV with a fixed flux limit (left, sensitivity $= 10^{-13}$ erg s^{-1} cm^{-2}) and the same rates as a function of sensitivity with a fixed field of view (right, FOV $= 1$ deg^2). As in the rest of this work, we limit the rates to $z \leq 1$ – which is why the number of observations per year eventually flattens with increasing sensitivity.
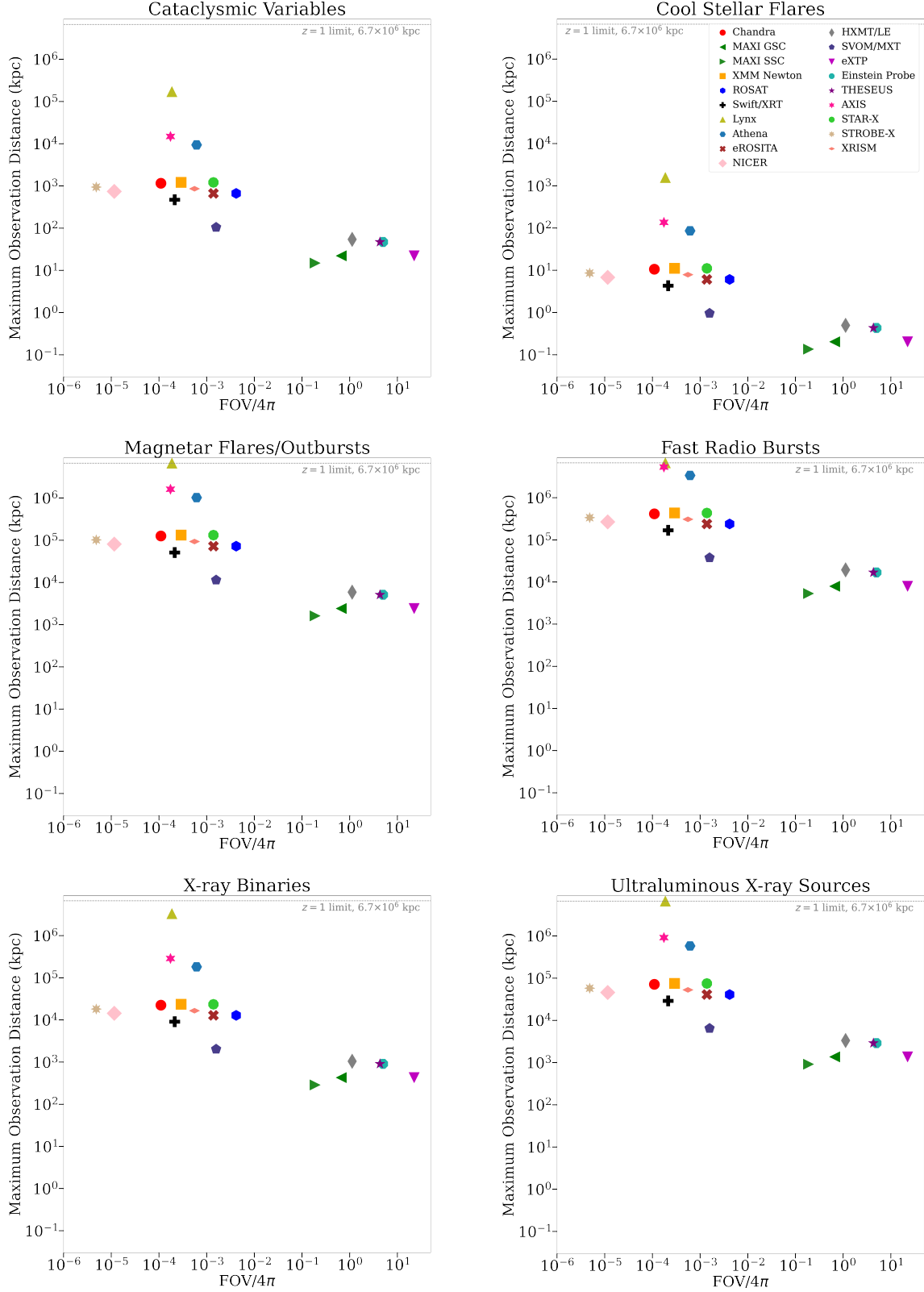
Figure 9. The maximum distance out to which each instrument can observe different classes of transient/variable vs. the normalized FOV (by the area of the sky). As in the rest of this work, we limit to $z \leq 1$ ($d_L = 6.7 \times 10^6$ kpc), which is shown by the gray dashed line.
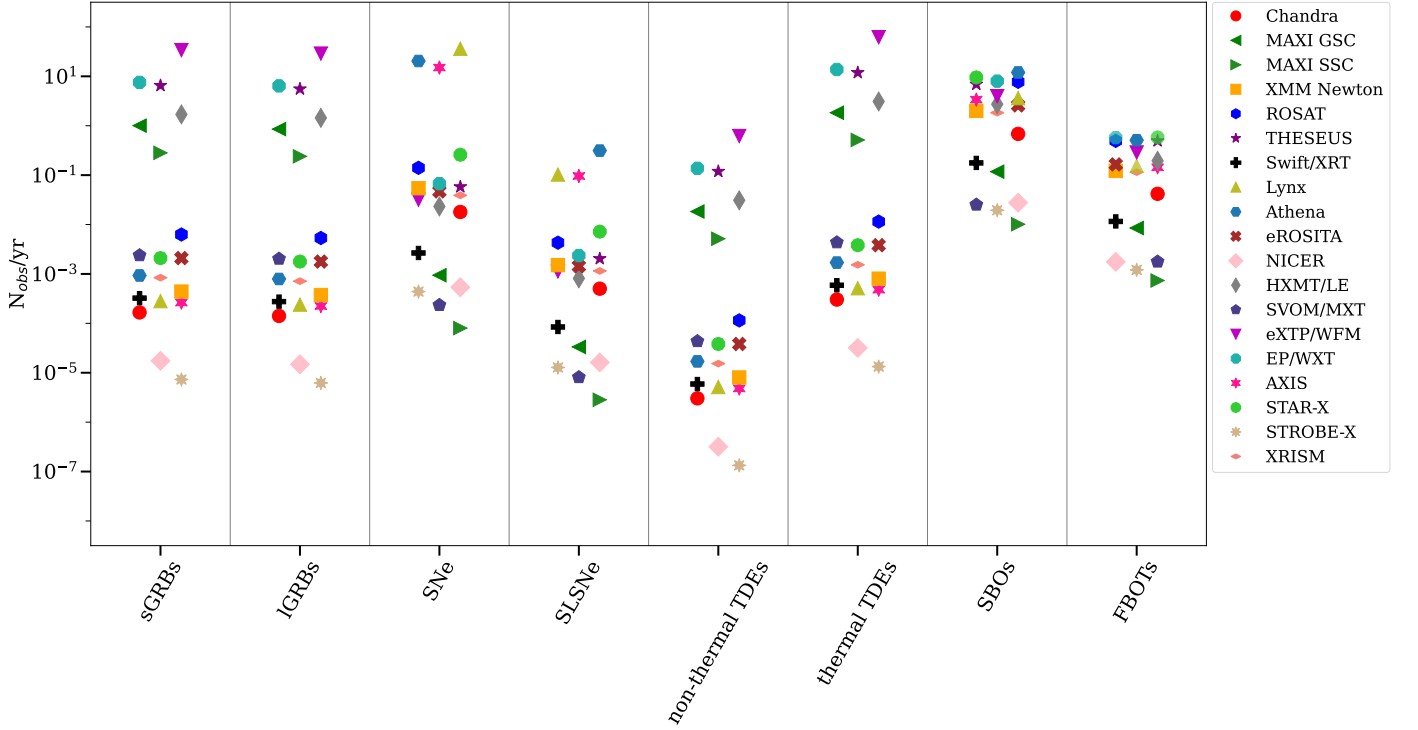
Figure 10. Estimates of the number of serendipitous observations expected per year for transients with a variety of different instruments based on the volumetric rates of the phenomena and the observing volume of each instrument. The comoving depth out to which each instrument can observe each class of phenomenon is calculated based on the peak observed luminosity of each phenomenon, making the assumption that we have already detected the most intrinsically luminous signal from each type of transient. We take rates from Stone & Metzger (2016), Coppejans et al. (2020), Margutti & Chornock (2021), and Ghirlanda & Salvaterra (2022). For the GRBs, both long and short, we apply a beaming correction assuming a jet opening angle $\sim 3°$. See Table 2 for more details. As with the rest of the paper, the number of expected observations per year is quoted out to $z = 1$, corresponding to $d_L \sim 6700$ Mpc or $d_{\mathrm{com}} \sim 3350$ Mpc.

Table A1. Gamma-Ray Bursts

Name	Type	T_{90} (s)	RA/Dec	z	Distance (kpc)	References
GRB980425A	subluminous	22.0^a	19:35:03.17 -52:50:46	0.0085	2.7×10^4	Pian et al. 2000; Kouveliotou et al. 2004
GRB031203A	subluminous	30^b	08:02:30.1 -39:51:03	0.105	4.9×10^5	Sazonov et al. 2004; Watson et al. 2004
GRB050509B	short	0.073	12:36:18.00 +29:01:24.0	0.225	1.1×10^6	Evans et al. 2007, 2009
GRB050724	short	3.00	16:24:44.400 -27:32:27.90	0.258	1.3×10^6	Evans et al. 2007, 2009
GRB051221A	short	1.400	21:54:48.626 +16:53:27.16	0.5465	3.2×10^6	Evans et al. 2007, 2009
GRB060218A	subluminous	2100	09:09:30.625 +33:08:20.16	0.0331	1.5×10^5	Evans et al. 2007, 2009
GRB061006	short	0.42	07:24:07.660 -79:11:55.10	0.438	2.4×10^6	Evans et al. 2007, 2009
GRB061210	short	85.0	09:38:05.270 +15:37:17.30	0.4095	2.3×10^6	Evans et al. 2007, 2009
GRB061217	short	0.210	10:41:39.320 -21:07:22.11	0.827	5.3×10^6	Evans et al. 2007, 2009
GRB070714B	short	3.0	03:51:22.30 +28:17:51.3	0.923	6.1×10^6	Evans et al. 2007, 2009
GRB070724A	short	0.4	01:51:14.08 -18:35:38.8	0.457	2.6×10^6	Evans et al. 2007, 2009
GRB071227	short	1.8	03:52:31.09 -55:59:03.3	0.383	2.1×10^6	Evans et al. 2007, 2009
GRB080905A	short	1.0	19:10:39.10 -18:51:55.4	0.1218	5.7×10^5	Evans et al. 2007, 2009
GRB090510A	short	0.3	22:14:12.60 -26:35:51.1	0.903	5.9×10^6	Evans et al. 2007, 2009
GRB100117A	short	0.3	00:45:04:56 -01:35:41.7	0.92	6.0×10^6	Evans et al. 2007, 2009
GRB100316D	subluminous	292.8	07:10:30.63 -56:15:19.7	0.059	2.7×10^5	Evans et al. 2007, 2009
GRB100816A	short	2.9	23:26:57.56 +26:34:42.6	0.8049	5.1×10^6	Evans et al. 2007, 2009
GRB101219A	short	0.6	04:58:20.45 -02:32:23.1	0.718	4.4×10^6	Evans et al. 2007, 2009
GRB101225A	ultralong	1088	00:00:47.48 +44:36:01.0	0.847	5.5×10^6	Evans et al. 2007, 2009
GRB141212A	short	0.30	02:36:29.95 +18:08:49.1	0.596	3.5×10^6	Evans et al. 2007, 2009
GRB141225A	long	40.24	09:15:06.79 +33:47:30.6	0.915	6.0×10^6	Evans et al. 2007, 2009
GRB150101B	short	0.08	12:32:04.98 -10:56:00.7	0.134	6.4×10^5	Evans et al. 2007, 2009
GRB150323A	long	149.6	08:32:42.74 +45:27:52.7	0.593	3.5×10^6	Evans et al. 2007, 2009
GRB150514A	long	10.8	04:59:30.46 -60:58:06.9	0.807	5.1×10^6	Evans et al. 2007, 2009
GRB150518A	subluminous	–	15:36:48.25 +16:19:47.3	0.256	1.3×10^6	Evans et al. 2007, 2009
GRB150727A	long	88	13:35:52.51 -18:19:32.5	0.313	1.6×10^6	Evans et al. 2007, 2009
GRB150818A	long	123.3	15:21:25.44 +68:20:31.3	0.282	1.5×10^6	Evans et al. 2007, 2009
GRB150821A	long	172.1	22:47:39.13 -57:53:38.1	0.755	4.7×10^6	Evans et al. 2007, 2009
GRB151027A	long	129.69	18:09:56.86 +61:21:11.9	0.81	5.2×10^6	Evans et al. 2007, 2009
GRB160131A	long	325	05:12:40.32 -07:02:59.5	0.972	6.5×10^6	Evans et al. 2007, 2009
GRB160314A	long	8.73	07:31:09.79 +16:59:57.3	0.726	4.9×10^6	Evans et al. 2007, 2009
GRB160425A	long	304.58	18:41:18.55 -54:21:36.1	0.555	3.2×10^6	Evans et al. 2007, 2009
GRB160623A	long	13.5	21:01:11.54 +42:13:15.4	0.367	2.0×10^6	Evans et al. 2007, 2009
GRB160624A	short	0.2	22:00:46.21 +29:38:37.8	0.483	2.7×10^6	Evans et al. 2007, 2009
GRB160804A	long	130	14:46:31.20 +09:59:55.9	0.736	4.6×10^3	Evans et al. 2007, 2009
GRB160821B	short	0.48	18:39:54.550 +62:23:30.35	0.16	7.7×10^5	Evans et al. 2007, 2009
GRB161129A	long	35.53	21:04:54.65 +32:08:05.4	0.645	3.9×10^6	Evans et al. 2007, 2009
GRB161219B	long	6.94	06:06:51.37 -26:47:29.7	0.1475	7.1×10^5	Evans et al. 2007, 2009
GRB170519A	long	216.4	10:53:42.50 +25:22:26.8	0.818	5.2×10^6	Evans et al. 2007, 2009
GRB170607A	long	23.0	00:29:27.82 +09:14:35.7	0.557	3.3×10^6	Evans et al. 2007, 2009
GRB170714A	ultralong	1000	02:17:23.97 +01:59:29.0	0.793	5.0×10^6	Evans et al. 2007, 2009
GRB170817A	short	2.0	13:09:48.085 -23:22:53.343	0.0099	4.3×10^4	Hajela et al. 2019, 2020
GRB171010A	long	70.3	04:26:19.42 -10:27:47.7	0.3285	1.7×10^6	Evans et al. 2007, 2009
GRB171205A	subluminous	189.4	11:09:39.49 -12:35:18.7	0.0368	1.6×10^5	Evans et al. 2007, 2009
GRB180404A	long	35.2	05:34:11.74 -37:10:04.8	1.000	6.7×10^6	Evans et al. 2007, 2009
GRB180703A	long	20.9	00:24:28.10 -67:18:17.9	0.6678	4.0×10^6	Evans et al. 2007, 2009
GRB180720B	long	51.1	00:02:06.86 -02:55:08.1	0.654	4.0×10^6	Evans et al. 2007, 2009
GRB180728A	long	8.68	16:54:15.60 -54:02:40.2	0.117	5.5×10^5	Evans et al. 2007, 2009
GRB190114C	long	361.5	03:38:01.18 -26:56:47.8	0.425	2.4×10^6	Evans et al. 2007, 2009
GRB190829A	long	63	02:58:10.50 -08:57:29.8	0.0785	3.6×10^5	Evans et al. 2007, 2009
GRB191019A	long	64.35	22:40:05.87 -17:19:40.8	0.248	1.3×10^6	Evans et al. 2007, 2009
GRB221009A	long	327	19:12:50.4 +19:43:48	0.151	7.2×10^5	Evans et al. 2007, 2009; de Ugarte Postigo et al. 2022

Table A2. Shock Breakouts

Name	Type	RA/Dec	Distance (kpc)	References
GRB980425A	stellar surface	19:35:03.17 -52:50:46.1	3.7×10^4	Pian et al. 2000; Kouveliotou et al. 2004
GRB031203A	stellar surface	08:02:30.1 -39:51:03	4.9×10^5	Sazonov et al. 2004; Watson et al. 2004
GRB060218A	stellar surface	03:21:39.670 +16:52:02.27	1.5×10^5	Evans et al. 2007, 2009
SN2008D (GRB080109A)	wind	09:09:30.625 +33:08:20.16	2.7×10^4	Soderberg et al. 2008
GRB100316D	stellar surface	07:10:30.63 -56:15:19.7	2.7×10^5	Evans et al. 2007, 2009
GRB150518A	stellar surface	15:36:48.25 +16:19:47.3	1.3×10^6	Evans et al. 2007, 2009
GRB171205A	stellar surface	11:09:39.49 -12:35:18.7	1.6×10^5	Evans et al. 2007, 2009

NOTE—Subluminous GRBs are considered candidates for stellar surface shock breakouts. We include them here under that assumption.
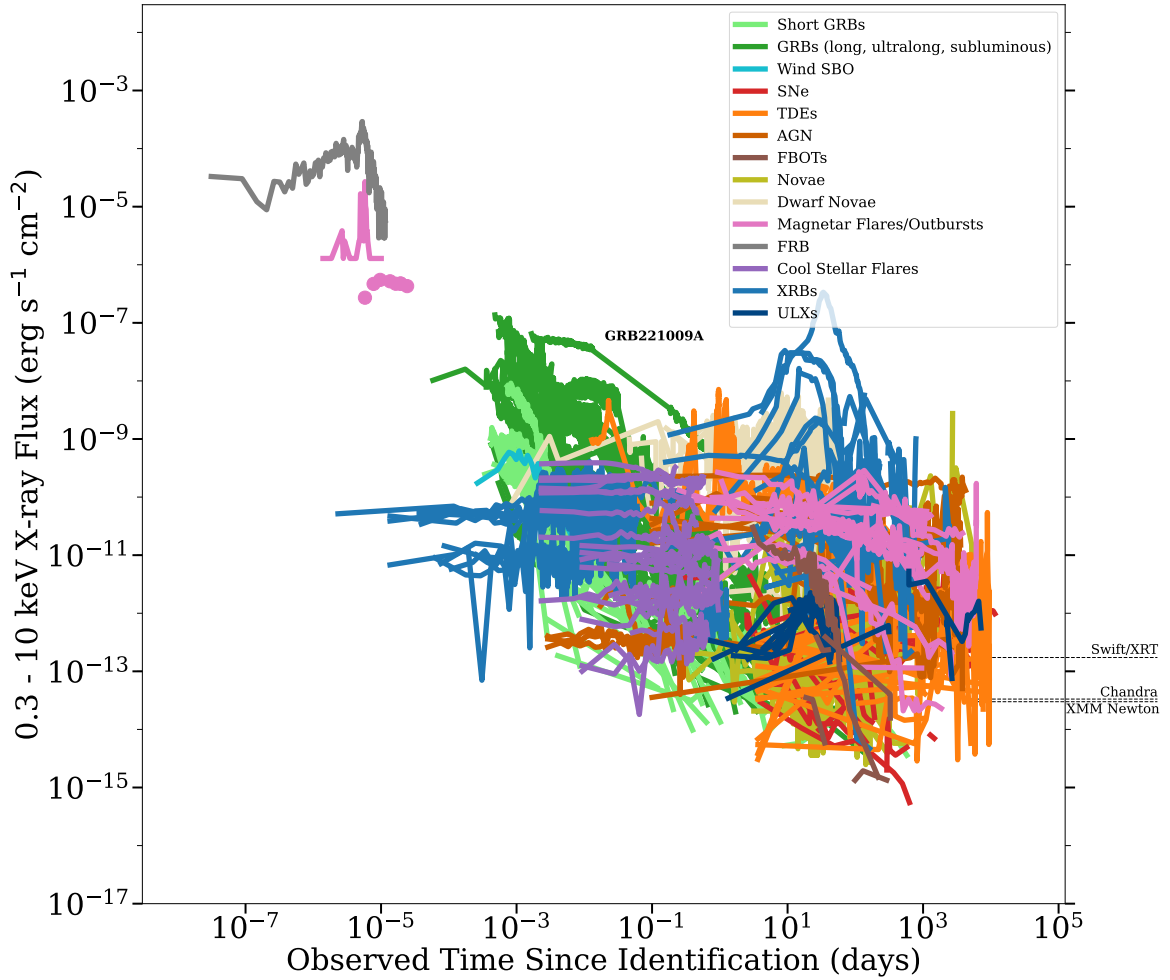
Figure 11. The duration-flux phase space of X-ray transient and variable phenomena. To demonstrate the limitations of current observatories, we mark the 0.3-10 keV flux limit for a handful of instruments, assuming a 1ks integration time.

Table A3. Supernovae

Name	Type	RA/Dec	Distance (kpc)	References
SN1978K	II	03:17:38.620 -66:33:03.40	4.5×10^3	Raffaella Margutti, Private Communication
SN1980K	IIL	20:35:30.07 +60:06:23.7	5.1×10^3	Soria & Perna 2008
SN1981K	II	12:18:59.42 +47:19:31.0	7.2×10^3	Immler et al. 2007b
SN1986J	IIn	02:22:31.33 +42:19:56.4	9.6×10^3	Raffaella Margutti, Private Communication
SN1987A	IIpec	05:35:28.020 -69:16:11.07	50	Haberl et al. 2006; Heng et al. 2008; Sturm et al. 2010
SN1993J	IIb	09:55:24.77 +69:01:13.7	2.6×10^3	Chandra et al. 2009
SN1995N	IIn	14:49:28.29 -10:10:14.0	2.4×10^4	Zampieri et al. 2005
SN1996cr	IIn	14:13:10.05 -65:20:44.8	3.8×10^3	Bauer et al. 2008
SN1998bw	Ib/c	19:35:03.17 -52:50:46.1	3.8×10^4	Kouveliotou et al. 2004
SN1999em	IIP	04:41:27.04 -02:51:45.2	7.8×10^3	Pooley et al. 2002
SN1999gi	IIP	10:18:16.66 +41:26:28.2	8.7×10^3	Schlegel 2001
SN2001em	Ib/c	21:42:23.61 +12:29:50.3	8.0×10^4	Pooley & Lewin 2004a
SN2001ig	II	22:57:30.69 -41:02:25.9	1.1×10^4	Schlegel & Ryder 2002
SN2002ap	Ib/c	01:36:23.85 +15:45:13.2	1.0×10^4	Soria et al. 2004
SN2002hh	II	20:34:44.29 +60:07:19.0	5.1×10^3	Pooley & Lewin 2002
SN2002hi	IIn	07:19:54.08 +17:58:18.8	1.8×10^5	Pooley & Lewin 2003
SN2003bg	Ic/pec	04:10:59.42 -31:24:50.3	1.9×10^4	Soderberg et al. 2006
SN2004dj	IIP	07:37:17.04 +65:35:57.8	3.2×10^3	Pooley & Lewin 2004b
SN2004et	II	20 35 25.33 +60 07 17.7	5.5×10^3	Misra et al. 2007
SN2005ip	IIn	09:32:06.42 +08:26:44.4	3.0×10^4	Immler & Pooley 2007
SN2005kd	IIn	04:03:16.88 +71:43:18.9	6.4×10^4	Immler et al. 2007c; Pooley et al. 2007
SN2006bp	IIP	11:53:55.74 +52:21:09.4	1.5×10^4	Immler et al. 2007e
SN2006jc	Ibc	09:17:20.78 +41:54:32.7	2.4×10^4	Immler et al. 2008
SN2006jd	IIb/IIn	08:02:07.43 +00:48:31.5	7.9×10^4	Immler et al. 2007a
SN2007pk	IIn	01:31:47.07 +33:36:54.1	7.1×10^4	Immler et al. 2007d
SN2008M	II	06:21:41.28 -59:43:45.4	3.7×10^4	Immler 2010
SN2008ax	IIb	12:30:40.80 +41:38:16.1	8.0×10^3	Roming et al. 2009
SN2008ij	II	18:19:51.81 +74:33:54.9	2.1×10^4	Immler et al. 2009
SN2009gj	IIb	00:30:28.56 -33:12:56.0	1.8×10^4	Immler & Russell 2009
SN2009mk	IIb	00:06:21.37 -41:28:59.8	2.1×10^4	Russell & Immler 2010
SN2010F	II	10:05:21.05 -34:13:21.0	3.9×10^4	Russell et al. 2010
SN2010jl	IIn	09:42:53.33 +09:29:41.8	4.9×10^4	Immler et al. 2010; Chandra et al. 2015
SN2011dh	IIb	13:30:05.106 +47:10:10.92	7.3×10^3	Soderberg et al. 2012
SN2011ja	IIP	13:05:11.12 -49:31:27.0	3.0×10^3	Chakraborti et al. 2013
PTF12dam	Ic/SL	14:24:46.20 +46:13:48.3	4.98×10^5	Margutti et al. 2018
SN2013by	IIL/IIn	16:59:02.43 -60:11:41.8	1.5×10^5	Margutti et al. 2013
SN2013ej	IIP/IIL	01:36:48.16 +15:45:31.0	9.6×10^3	Chakraborti et al. 2016
SN2014C	Ib/IIn	22:37:05.60 +34:24:31.9	1.5×10^4	Brethauer et al. 2022
SN2015L (ASASSN-15lh)	I/SL	22:02:15.45 -61:39:34.6	1.2×10^6	Margutti et al. 2017
SN2018gk	IIb/SL	16:35:53.908 +40:01:58.31	5.0×10^5	Bose et al. 2020
SN2019ehk	Ca-rich	12:22:56.130 +15:49:33.60	1.6×10^4	Jacobson-Galán et al. 2020
SN2021gno	Ca-rich	12:12:10.29 +13:14:57.04	3.05×10^4	Jacobson-Galán et al. 2022

NOTE—Type "SL" denotes superluminous supernovae.

Table A4. Tidal Disruption Events and Active Galactic Nuclei

Name	Type	RA/Dec	Distance (kpc)	References
PKS 2155-304	AGN	21:58:52.07 -30:13:32.1	5.4×10^5	Auchettl et al. 2018
3C 273	AGN	12:29:06.70 +02:03:08.6	7.6×10^5	Auchettl et al. 2018
NGC 4395	AGN	12:25:48.86 +33:32:48.7	4.7×10^3	Auchettl et al. 2018
3C 279	AGN	12:56:11.17 -05:47:21.5	3.1×10^6	Auchettl et al. 2018
3C 345	AGN	16:42:58.81 +39:48:37.0	3.5×10^6	Auchettl et al. 2018
MKN 335	AGN	00:06:19.54 +20:12:10.6	1.1×10^5	Auchettl et al. 2018
NGC 3227	AGN	10:23:30.57 +19:51:54.3	1.6×10^4	Auchettl et al. 2018
CGC 229-10 (Zw 299-015)	AGN	16:41:09.034 +61:19:34.74	8.7×10^4	Auchettl et al. 2018
PS10jh	thermal TDE	16:09:28.296 53:40:23.52	8.2×10^5	Gezari et al. 2012; Auchettl et al. 2017
1H0707-495	AGN	07:08:41.49 -49:33:06.3	1.8×10^5	Auchettl et al. 2018
ASASSN-14ae	thermal TDE	11:08:40.11 +34:05:52.4	2.0×10^5	Holoien et al. 2014; Auchettl et al. 2017
ASASSN-14li	thermal TDE	12:48:15.22 +17:46:26.5	9.0×10^4	Miller et al. 2015; Brown et al. 2017
				Auchettl et al. 2017; Bright et al. 2018
ASASSN-15oi	thermal TDE	20:39:09.096 -30:45:20.71	2.2×10^5	Auchettl et al. 2017; Holoien et al. 2018
Swift 1644+57	non-thermal TDE	16:44:49.3 +57:34:51	1.9×10^6	Mangano et al. 2016; Auchettl et al. 2017
ASASSN-19bt	non-thermal TDE	07:00:11.410 -66:02:25.16	1.15×10^5	Holoien et al. 2019
Swift J2058.4+0516[a]	non-thermal TDE	20:58:19.898 +05:13:32.25	1×10^7	Auchettl et al. 2017
SDSS J131122.15-012345.6	thermal TDE	13:11:22.154 -01:23:45.61	9.0×10^5	Auchettl et al. 2017
SDSS J132341.97+482701.3	thermal TDE	13:23:41.973 +48:27:01.26	4.0×10^5	Auchettl et al. 2017
SDSS J1201+3003	thermal TDE	12:01:36.028 +30:03:05.52	7.1×10^5	Auchettl et al. 2017
WINGS J1348	thermal TDE	13:48:51.1 +26:35:05.7	2.8×10^5	Auchettl et al. 2017
RBS 1032	thermal TDE	11:47:26.73 +49:42:57.3	1.1×10^5	Auchettl et al. 2017
3XMM J1521+0749	thermal TDE	11:47:26.70 +49:42:57.8	8.9×10^5	Auchettl et al. 2017
GSN 069	AGN/QPE	01:19:08.66 -34:11:30.5	7.86×10^4	Miniutti et al. 2019
2MASX J0249	thermal TDE	02:49:17.32 -04:12:52.20	8.0×10^4	Auchettl et al. 2017
IGR J17361-4441	thermal TDE	17:36:17.42 -44:44:05.98	1.8×10^5	Auchettl et al. 2017
NGC 247	thermal TDE	00:47:08.55 -20:45:37.44	2240	Auchettl et al. 2017
OGLE 16aaa	thermal TDE	01:07:20.88 -64:16:20.70	8.1×10^5	Auchettl et al. 2017
PTF-10iya	thermal TDE	14:38:40.98 +37:39:33.45	1.2×10^6	Auchettl et al. 2017
XMMSL1 J0740-85	thermal TDE	07:40:08.09 -85:39:31.30	7.4×10^5	Auchettl et al. 2017

[a]Though Swift J2058.4+0516 is at $z \sim 1$, we include its light curve anyway due to the relative paucity of non-thermal TDE observations and the uncertainty on its distance estimate.

Table A5. Fast Blue Optical Transients

Name	RA/Dec	Distance (kpc)	References
CSS161010	04:58:34.396 -08:18:03.95	1.5×10^5	Coppejans et al. 2020
AT2018cow	16:16:00.2242 +22:16:04.890	6.0×10^4	Margutti et al. 2019
AT2020xnd	22:20:02.04 -02:50:25.1	1.2×10^6	Bright et al. 2022
AT2020mrf	15:47:54.18 +44:29:07.16	6.37×10^5	Yao et al. 2022
AT2022tsd	03:20:10.863 +08:44:55.63	1.3×10^6	Schulze et al. 2022; Matthews et al. 2022

Table A6. Cataclysmic Variables

Name	Type	RA/Dec	Distance (kpc)	References
V838 Her	Nova	18:46:31.56 +12:14:00.7	3.4	Mukai et al. 2008
V1974 Cyg	Nova	20:30:31.61 +52:37:51.3	1.9	Mukai et al. 2008
V351 Pup	Nova	08:11:38.38 -35:07:30.4	4.7	Mukai et al. 2008
V382 Vel	Nova	10:44:48.39 -52:25:30.7	1.7	Mukai et al. 2008
N LMC 2000[a]	Nova	05:25:01.63 -70:14:17.4	55	Mukai et al. 2008
V4633 Sgr	Nova	18:21:40.49 -27:31:37.3	8.9	Mukai et al. 2008
N LMC 2005[a]	Nova	05:10:32.68 -69:12:35.7	55	Mukai et al. 2008
V5116 Sgr	Nova	18:17:50.77 -30:26:31.3	11.3	Mukai et al. 2008
V1663 Aql	Nova	19:05:12.50 +05:14:12.0	5.5	Mukai et al. 2008
V1188 Sco	Nova	17:44:21.59 -34:16:35.7	7.5	Mukai et al. 2008
V477 Sct	Nova	18:38:42.93 -12:16:15.6	11	Mukai et al. 2008
V476 Sct	Nova	18:32:04.75 -06:43:34.3	4	Mukai et al. 2008
V382 Nor	Nova	16:19:44.74 -51:34:53.1	13.8	Mukai et al. 2008
RS Oph	Nova	17:50:13.2 -06:42:28.5	1.6	Page et al. 2020
V2362 Cyg	Nova	21:11:32.342 +44:48:03.67	7.2 - 15.8	Poggiani 2009; Page et al. 2020
V1280 Sco	Nova	16:57:40.91 -32:20:36.4	1.6	Chesneau et al. 2008; Page et al. 2020
V1281 Sco	Nova	16:56:59.35 -35:21:50.2	25.9	Kantharia 2017; Page et al. 2020
V458 Vul	Nova	19:54:24.61 +20:52:52.6	8.5	Page et al. 2020
V597 Pup	Nova	08:16:17.953 -34:15:25.19	3	Worpel et al. 2020; Page et al. 2020
V2468 Cyg	Nova	19:58:33.57 +29:52:11.6	5.6	Raj et al. 2015; Page et al. 2020
V2491 Cyg	Nova	19:43:01.977 +32:19:13.55	10.5 - 14	Darnley et al. 2011; Page et al. 2020
HV Cet (CSS081007)	Nova	03:05:58.53 +05:47:15.7	4.45	Page et al. 2020
LMC 2009a	Nova	05:04:44.20 -66:40:11.6	50	Page et al. 2020
V2672 Oph	Nova	17:38:19.72 -26:44:13.7	19	Munari et al. 2011; Page et al. 2020
KT Eri	Nova	04:47:54.201 -10:10:42.96	6.3	Raj et al. 2013; Page et al. 2020
U Sco	Nova	16:22:30.778 -17:52:43.16	12	Schaefer 2010; Page et al. 2020
V407 Cyg	Nova	21:02:09.8 +45:46:32.7	2.7	Page et al. 2020
T Pyx	Nova	09:04:41.506 -32:22:47.50	3.185	Schaefer 2018; Page et al. 2020
LMC 2012	Nova	04:54:56.852 -70:26:56.40	50	Page et al. 2020
V959 Mon	Nova	06:39:38.599 +05:53:52.88	1.4	Page et al. 2020; Li et al. 2020a
SMC 2012	Nova	00:32:34.384 -74:20:14.55	61	Page et al. 2020
V339 Del	Nova	20:23:30.686 +20:46:03.78	2.1	Page et al. 2020; Li et al. 2020a
V1369 Cen	Nova	13:54:45.363 -59:09:04.17	2.0	Page et al. 2020; Li et al. 2020a
V745 Sco	Nova	17:55:22.227 -33:14:58.56	7.8	Schaefer 2010; Page et al. 2020
V1534 Sco	Nova	17:15:46.83 -31:28:30.3	8.8	Hachisu & Kato 2018; Page et al. 2020
V1535 Sco	Nova	17:03:26.171 -35:04:17.82	8.5	Linford et al. 2017; Page et al. 2020
V5668 Sgr	Nova	18:37:39.9 -29:04:03	2.0	Page et al. 2020; Li et al. 2020a
LMC 1968-12a	Nova	05:09:58.40 -71:39:52.7	50	Page et al. 2020
V407 Lup	Nova	15:29:01.820 -44:49:40.89	∼ 10	Aydi et al. 2018; Page et al. 2020
SMCN 2016-10a	Nova	01:06:03.27 -74:47:15.8	61	Page et al. 2020
V549 Vel	Nova	08:50:29.62 -47:45:28.3	0.560	Page et al. 2020; Li et al. 2020a
SS Cyg	Dwarf Nova	21:42:42.80 +43:35:09.9	0.115	Pala et al. 2020; Wheatley et al. 2003; McGowan et al. 2004
GW Lib	Dwarf Nova	15:19:55.33 -25:00:24.6	0.113	Pala et al. 2020; Byckling et al. 2009; Neustroev et al. 2018
SSS J122221.7-311525	Dwarf Nova	12:22:21.67 -31:15:23.8	0.275	Neustroev et al. 2018

NOTE—We include only the dwarf novae with well-observed X-ray brightenings during their optical outbursts.

[a] We quote the 55 kpc distance assumed by Mukai et al. (2008) since these light curves are from that paper and presented as luminosity vs. time. Other novae in the LMC are listed with a more recently revised distance (Pietrzyński et al. 2013) as those data were initially presented as flux vs. time.

Table A7. Magnetar Flares/Outbursts + FRBs

Name	Type	RA/Dec	Distance (kpc)	References
1E161348-5055	Outburst	16:17:33.000 -51:02:00.00	3.3	Rea et al. 2016; Esposito et al. 2019
SGR 1900+14	IF/SB	19:07:13.0 +09:19:34	10.4	Case & Bhattacharya 1998; Israel et al. 2008
SGR 1627-41	Outburst	16:35:52.0 -0.47:35:12	11	Coti Zelati et al. 2018
1E2259+586	Outburst	23:01:08.14 +58:52:44.5	3.2	Coti Zelati et al. 2018
XTE J1810-197	Outburst	18:09:51.07 -19:43:51.8	3.5	Coti Zelati et al. 2018
SGR 1806-20	Outburst	18:08:39.32 -20:24:40.1	8.7	Coti Zelati et al. 2018
CXOU J1647-4552	Outburst	16:47:10.18 -45:52:16.7	4	Coti Zelati et al. 2018
SGR 0501+4516	Outburst	05:01:08.0 +45:16:31	1.5	Coti Zelati et al. 2018
1E1547.0-5408	Outburst	15:50:54.18 -54:18:23.9	4.5	Coti Zelati et al. 2018
SGR 0418+5729	Outburst	04:18:33.867 +57:32:22.91	2	Coti Zelati et al. 2018
SGR 1833-0832	Outburst	18:33:46.0 -08:32:13	10	Coti Zelati et al. 2018
Swift J1822.3-1606	Outburst	18:22:18.32 -16:04:27.2	1.6	Coti Zelati et al. 2018
Swift J1834.9-0846	Outburst	18:34:52.768 -08:45:40.83	4.2	Coti Zelati et al. 2018
1E1048.1-5937	Outburst	10:50:08.93 -59:53:19.9	9	Coti Zelati et al. 2018
SGR J1745-2900	Outburst	17:45:40.1640 -29:00:29.818	8.3	Coti Zelati et al. 2018
SGR 1935+2154 (FRB 200428)[a]	FRB	19:34:55.68 +21:53:48.2	4.4	Li et al. 2021
SGR 1935+2154	IF/SB			Matsuoka et al. 2009; Sugawara et al. 2020

Note—As with the other variable classes, one listed object may correspond to multiple light curves within our X-ray phase space. To remain consistent with our discussion in Section 2.7, we categorize magnetar transience as either intermediate flare/short burst (IF/SB in the table) or outburst. Quiescent behavior is shown for the listed outbursts, with L_x taken from Olausen & Kaspi (2014).

[a]SGR 1935+2154 is believed to be a fast radio burst X-ray counterpart with a magnetar progenitor. For that reason, we include it with our sample of magnetar flares and outbursts. These data (both the IF/SB and FRB counterpart) are from the same burst forest in April 2020 for direct comparison. We adopt a distance of 4.4 kpc from Mereghetti et al. (2020).

Table A8. Cool Stellar Flares

Name	RA/Dec	Distance (kpc)	References
UY Scl	00:14:45.752 -39:14:35.57	0.1372	Pye et al. 2015
HD 1165	00:16:52.517 +81:39:49.08	0.0332	Pye et al. 2015
HD 14716	02:16:03.509 -73:50:43.11	0.062	Pye et al. 2015
CC Eri	02:34:22.566 -43:47:46.87	0.0116	Pye et al. 2015
CD-53 544	02:41:46.836 -52:59:52.40	0.028	Pye et al. 2015
SDSS J033815.04+002926.0	03:38:15.040 +00:29:26.13	0.7099	Pye et al. 2015
V471 Tau	03:50:24.966 +17:14:47.43	0.0441	Pye et al. 2015
2MASS J04072181-1210033	04:07:21.808 -12:10:03.32	0.3957	Pye et al. 2015
V410 Tau	04:18:31.108 +28:27:16.16	0.0982	Pye et al. 2015
T Tau	04:21:59.432 +19:32:06.44	0.1825	Pye et al. 2015
HD 285845	04:31:25.125 +18:16:16.73	0.090	Pye et al. 2015
HD 283810	04:40:09.228 +25:35:32.61	0.060	Pye et al. 2015
HD 268974	05:05:26.980 -67:43:13.52	0.9174	Pye et al. 2015
AB Dor	05:28:44.892 -65:26:55.29	0.0152	Pye et al. 2015
SV Cam	06:41:19.082 +82:16:02.44	0.088	Pye et al. 2015
pi.01 UMa	08:39:11.704 +65:01:15.27	0.0144	Pye et al. 2015
2MASS J13141103-1620235	13:14:11.020 -16:20:24.11	0.5161	Pye et al. 2015
1RXS J231628.7+790531	23:16:30.715 +79:05:36.28	0.055	Pye et al. 2015

Note—As with the progenitors of other classes of recurrent outburst, individual flares are shown separately in our X-ray phase space, so some of the objects listed may correspond to a number of unique light curves.

Table A9. X-ray Binary Outbursts and Ultraluminous X-ray Sources

Name	Type	RA/Dec	Distance (kpc)	Reference
4U 0352-309 (X Persei)	HMXRB	03:55:23.077 +31:02:45.05	1	La Palombara & Mereghetti 2007
XMMU J004243.6+412519	ULX	00:42:43.68 +41:25:18.6	778	Middleton et al. 2013
RX J0209.6-7427	HMXRB	02:09:33.85 -74:27:12.5	55	Vasilopoulos et al. 2020b
PSR J1023+0038[a]	LMXRB	10:23:47.684 +00:38:41.01	1.37	Bogdanov et al. 2015
IGR J01217-7257 (SXP 2.16)	HMXRB	01:21:40.6 -72:57:21.9	62	Boon et al. 2017; Vasilopoulos et al. 2017a
SXP 15.6	HMXRB	00:48:55.360 -73:49:45.70	62	Vasilopoulos et al. 2017b
CG X-1	ULX	14:13:12.21 -65:20:13.7	4200	Qiu et al. 2019
M51 ULX-7	ULX	13:30:01.02 47:13:43.8	8580	Vasilopoulos et al. 2020a
NGC 925 ULX-3	ULX	02:27:20.18 +33:34:12.84	9560	Earnshaw et al. 2020
Aql X-1[b]	LMXRB	19:11:16.057 +00:35:05.88	~ 5	López-Navas et al. 2020
GX 339-4[b]	LMXRB	17:02:49.381 -48:47:23.16	8	Kong et al. 2000; Corbel et al. 2013
MAXI J1659-152	LMXRB	16:59:01.680 -15:15:28.73	6	Jonker et al. 2012
4U J1907+09	HMXRB	19:09:40.8 +09:48:25	5	Ferrigno et al. 2022
IGR J16393-4643	HMXRB	16:39:05.5 -46:42:14	12	Ferrigno et al. 2022
IGR J17503-2636	HMXRB	17:50:18.06 -26:36:16.7	10	Ferrigno et al. 2022
IGR J19140+0951	HMXRB	19:14:04.23 +09:52:58.4	2.8	Ferrigno et al. 2022
Swift J0243.6+6124	HMXRB	02:43:40.43 +61:26:03.8	7	Wilson-Hodge et al. 2018; Chatzis et al. 2022
RX J0520.5-6932	HMXRB	05:20:30.90 -69:31:55.0	50	Vasilopoulos et al. 2014
SMC X-2	HMXRB	00:54:33.43 -73:41:01.3	62	Lutovinov et al. 2017
SMC X-3	HMXRB	00:52:05.63 -72:26:04.2	62	Koliopanos & Vasilopoulos 2018
XMMU J053108.3-690923	HMXRB	05:31:08.44 -69:09:23.5	50	Vasilopoulos et al. 2018; Maitra et al. 2021
XTE J1859+226	LMXRB	18:58:41.580 +22:39:29.40	6.3	Hameury et al. 2003; Gallo et al. 2008
GS 2023+338	LMXRB	20:24:03.825 +33:52:01.96	3.5	Kong et al. 2000
4U 1630-47	LMXRB	16:34:01.610 -47:23:34.80	10	Kong et al. 2000
CXOGLB J173617.6-444416	LMXRB	17:36:17.686 -44:44:16.72	9.9	Maxwell et al. 2012
CXOGLB J173616.9-444409	LMXRB	17:36:16.937 -44:44:09.85	9.9	Maxwell et al. 2012
CXOGLB J173617.3-444408	LMXRB	17:36:17.329 -44:44:08.23	9.9	Maxwell et al. 2012
CXOGLB J173618.1-444359	LMXRB	17:36:18.188 -44:43:59.47	9.9	Maxwell et al. 2012
CXOGLB J173617.5-444357	LMXRB	17:36:17.520 -44:43:57.13	9.9	Maxwell et al. 2012
IGR J17544-2619	HMXRB	17:54:25.284 -26:19:52.62	3.5, 3.6	in't Zand 2005; Sidoli et al. 2008
IGR J08408–4503	HMXRB	08:40:47.792 -45:03:32.23	2.7	Leyder et al. 2007
KS 1741-293	HMXRB	17:44:51.63 -29:20:42.8	~ 8.5	Sakano et al. 2002
GRS 1741.9-2853	HMXRB	17:45:02.33 -28:54:49.7	~ 8.5	Sakano et al. 2002
IGR J16479-4514	HMXRB	16:48:06.56 -45:12:06.8	4.9	Sidoli et al. 2008
XTE J1739-302	HMXRB	17:39:11.552 -30:20:37.78	2.7	Sidoli et al. 2008
IGR J18410-0535	HMXRB	18:41:00.43 -05:35:46.5	5	Sidoli et al. 2008
CI Cam [c]	ULX	04:19:42.135 +55:59:57.71	1-10	Bartlett et al. 2019

NOTE—Objects with light curves shown in the X-ray phase space are above the horizontal line. Below the line, we list objects for which we show the quiescent behavior. As with other variable phenomena that show recurrent outbursts and flares, some objects may correspond to a number of unique light curves.

[a] These data are not shared in the GitHub repository.

[b] The light curves *and* quiescent behavior of Aql X-1 and GX 339-4 are shown in the X-ray phase space.

[c] We note that CI Cam is a ULX as long as it is at a distance > 8 kpc.

Table A10. Unclassified X-ray Sources

Name	RA/Dec	z	Distance (kpc)	Reference
XRT 000519	12:25:31.64 +13:03:58.8	0.23 - 1.5	1.62×10^4	Jonker et al. 2013
			1.1×10^6	
			1.11×10^7	
XRT 110103[a]	14:08:28.89 -27:03:29.4	-	9.49×10^4	Glennie et al. 2015
XRT 120830[a]	23:52:12.19 -46:43:43.3	-	0.08	Glennie et al. 2015
CDF-S XT1[b]	03:32:38.77 -27:51:33.67	0.3 - 2.23	1.6×10^6	Bauer et al. 2017
			1.81×10^7	
EXMM 023135.0-603743	02:31:34.9 -60:37:43.3	0.092	4.35×10^5	Novara et al. 2020

[a] These data are digitized (Rohatgi 2019) and so are not included in the GitHub repository of light curves from this paper.

[b] See Quirola-Vásquez et al. (2022) for data.

REFERENCES

Abbott, B. P., Abbott, R., Abbott, T. D., et al. 2017, ApJL, 848, L12, doi: 10.3847/2041-8213/aa91c9

Alexander, K. D., van Velzen, S., Horesh, A., & Zauderer, B. A. 2020, SSRv, 216, 81, doi: 10.1007/s11214-020-00702-w

Alp, D., & Larsson, J. 2020, ApJ, 896, 39, doi: 10.3847/1538-4357/ab91ba

Amati, L., O'Brien, P. T., Götz, D., et al. 2021, Experimental Astronomy, 52, 183, doi: 10.1007/s10686-021-09807-8

Angelini, L., & Verbunt, F. 1989, MNRAS, 238, 697, doi: 10.1093/mnras/238.3.697

Arcavi, I., Wolf, W. M., Howell, D. A., et al. 2016, ApJ, 819, 35, doi: 10.3847/0004-637X/819/1/35

Arzoumanian, Z., Gendreau, K. C., Baker, C. L., et al. 2014, in Society of Photo-Optical Instrumentation Engineers (SPIE) Conference Series, Vol. 9144, Space Telescopes and Instrumentation 2014: Ultraviolet to Gamma Ray, ed. T. Takahashi, J.-W. A. den Herder, & M. Bautz, 914420, doi: 10.1117/12.2056811

Astropy Collaboration, Robitaille, T. P., Tollerud, E. J., et al. 2013, A&A, 558, A33, doi: 10.1051/0004-6361/201322068

Astropy Collaboration, Price-Whelan, A. M., Sipőcz, B. M., et al. 2018, AJ, 156, 123, doi: 10.3847/1538-3881/aabc4f

Auchettl, K., Guillochon, J., & Ramirez-Ruiz, E. 2017, ApJ, 838, 149, doi: 10.3847/1538-4357/aa633b

Auchettl, K., Ramirez-Ruiz, E., & Guillochon, J. 2018, ApJ, 852, 37, doi: 10.3847/1538-4357/aa9b7c

Aydi, E., Orio, M., Beardmore, A. P., et al. 2018, MNRAS, 480, 572, doi: 10.1093/mnras/sty1759

Balberg, S., & Loeb, A. 2011, MNRAS, 414, 1715, doi: 10.1111/j.1365-2966.2011.18505.x

Barcons, X., Barret, D., Decourchelle, A., et al. 2012, arXiv e-prints, arXiv:1207.2745. https://arxiv.org/abs/1207.2745

Bartlett, E. S., Clark, J. S., & Negueruela, I. 2019, A&A, 622, A93, doi: 10.1051/0004-6361/201834315

Bauer, F. E., Dwarkadas, V. V., Brandt, W. N., et al. 2008, ApJ, 688, 1210, doi: 10.1086/589761

Bauer, F. E., Treister, E., Schawinski, K., et al. 2017, Monthly Notices of the Royal Astronomical Society, 467, 4841–4857, doi: 10.1093/mnras/stx417

Bochenek, C. D., Ravi, V., Belov, K. V., et al. 2020, Nature, 587, 59, doi: 10.1038/s41586-020-2872-x

Bogdanov, S., Archibald, A. M., Bassa, C., et al. 2015, ApJ, 806, 148, doi: 10.1088/0004-637X/806/2/148

Boon, C. M., Bird, A. J., Coe, M. J., et al. 2017, MNRAS, 466, 1149, doi: 10.1093/mnras/stw3169

Bose, S., Dong, S., Kochanek, C. S., et al. 2020, ASASSN-18am/SN 2018gk : An overluminous Type IIb supernova from a massive progenitor. https://arxiv.org/abs/2007.00008

Brethauer, D., Margutti, R., Milisavljevic, D., et al. 2022, arXiv e-prints, arXiv:2206.00842. https://arxiv.org/abs/2206.00842

Briel, U. G., Aschenbach, B., Hasinger, G., et al. 1996, The ROSAT Users' Handbook

Bright, J. S., Fender, R. P., Motta, S. E., et al. 2018, MNRAS, 475, 4011, doi: 10.1093/mnras/sty077

Bright, J. S., Margutti, R., Matthews, D., et al. 2022, ApJ, 926, 112, doi: 10.3847/1538-4357/ac4506

Brown, J. S., Holoien, T. W. S., Auchettl, K., et al. 2017, MNRAS, 466, 4904, doi: 10.1093/mnras/stx033

Burrows, D. N., Hill, J. E., Nousek, J. A., et al. 2005, SSRv, 120, 165, doi: 10.1007/s11214-005-5097-2

Byckling, K., Osborne, J. P., Wheatley, P. J., et al. 2009, MNRAS, 399, 1576, doi: 10.1111/j.1365-2966.2009.15378.x

Carter, B., & Luminet, J. P. 1982, Nature, 296, 211, doi: 10.1038/296211a0

—. 1983, A&A, 121, 97

Case, G. L., & Bhattacharya, D. 1998, ApJ, 504, 761, doi: 10.1086/306089

Chakraborti, S., Ray, A., Smith, R., et al. 2013, ApJ, 774, 30, doi: 10.1088/0004-637X/774/1/30

—. 2016, ApJ, 817, 22, doi: 10.3847/0004-637X/817/1/22

Chandra, P., Chevalier, R. A., Chugai, N., Fransson, C., & Soderberg, A. M. 2015, The Astrophysical Journal, 810, 32, doi: 10.1088/0004-637x/810/1/32

Chandra, P., Dwarkadas, V. V., Ray, A., Immler, S., & Pooley, D. 2009, ApJ, 699, 388, doi: 10.1088/0004-637X/699/1/388

Chandra X-ray Center, Chandra Project Science, MSFC, & Chandra IPI Teams. 2021, The Chandra Proposers' Observatory Guide, Tech. Rep. 24

Chatzis, M., Petropoulou, M., & Vasilopoulos, G. 2022, MNRAS, 509, 2532, doi: 10.1093/mnras/stab3098

Chen, G., Ravi, V., & Lu, W. 2020, ApJ, 897, 146, doi: 10.3847/1538-4357/ab982b

Chesneau, O., Banerjee, D. P. K., Millour, F., et al. 2008, A&A, 487, 223, doi: 10.1051/0004-6361:200809485

Chevalier, R. A., & Fransson, C. 2017, in Handbook of Supernovae, ed. A. W. Alsabti & P. Murdin, 875, doi: 10.1007/978-3-319-21846-5_34

Coppejans, D. L., Margutti, R., Terreran, G., et al. 2020, ApJL, 895, L23, doi: 10.3847/2041-8213/ab8cc7

Corbel, S., Coriat, M., Brocksopp, C., et al. 2013, MNRAS, 428, 2500, doi: 10.1093/mnras/sts215

Coti Zelati, F., Rea, N., Pons, J. A., Campana, S., & Esposito, P. 2018, MNRAS, 474, 961, doi: 10.1093/mnras/stx2679

Darnley, M. J., Ribeiro, V. A. R. M., Bode, M. F., & Munari, U. 2011, A&A, 530, A70, doi: 10.1051/0004-6361/201016038

De Luca, A., Salvaterra, R., Belfiore, A., et al. 2021, A&A, 650, A167, doi: 10.1051/0004-6361/202039783

de Ugarte Postigo, A., Izzo, L., Pugliese, G., et al. 2022, GRB Coordinates Network, 32748, 1

Dong, F. A., & CHIME/FRB Collaboration. 2022, The Astronomer's Telegram, 15681, 1

Drout, M. R., Chornock, R., Soderberg, A. M., et al. 2014, ApJ, 794, 23, doi: 10.1088/0004-637X/794/1/23

Earnshaw, H. P., Heida, M., Brightman, M., et al. 2020, ApJ, 891, 153, doi: 10.3847/1538-4357/ab77b8

Eftekhari, T., Berger, E., Metzger, B. D., et al. 2022, ApJ, 935, 16, doi: 10.3847/1538-4357/ac7ce8

Esposito, P., Rea, N., & Israel, G. L. 2021, in Astrophysics and Space Science Library, Vol. 461, Astrophysics and Space Science Library, ed. T. M. Belloni, M. Méndez, & C. Zhang, 97–142, doi: 10.1007/978-3-662-62110-3_3

Esposito, P., De Luca, A., Turolla, R., et al. 2019, A&A, 626, A19, doi: 10.1051/0004-6361/201935412

Evans, P. A., Page, K. L., Bearmore, A. P., et al. 2022, arXiv e-prints, arXiv:2208.14478. https://arxiv.org/abs/2208.14478

Evans, P. A., Beardmore, A. P., Page, K. L., et al. 2007, A&A, 469, 379, doi: 10.1051/0004-6361:20077530

—. 2009, MNRAS, 397, 1177, doi: 10.1111/j.1365-2966.2009.14913.x

Evans, P. A., Page, K. L., Osborne, J. P., et al. 2020, ApJS, 247, 54, doi: 10.3847/1538-4365/ab7db9

Ferrigno, C., Bozzo, E., & Romano, P. 2022, A&A, 664, A99, doi: 10.1051/0004-6361/202243294

Fertig, D., Mukai, K., Nelson, T., & Cannizzo, J. K. 2011, PASP, 123, 1054, doi: 10.1086/661949

Fong, W., Berger, E., Margutti, R., & Zauderer, B. A. 2015, ApJ, 815, 102, doi: 10.1088/0004-637X/815/2/102

Gallo, E., Homan, J., Jonker, P. G., & Tomsick, J. A. 2008, ApJL, 683, L51, doi: 10.1086/591230

Gezari, S., Chornock, R., Rest, A., et al. 2012, Nature, 485, 217, doi: 10.1038/nature10990

Ghirlanda, G., & Salvaterra, R. 2022, ApJ, 932, 10, doi: 10.3847/1538-4357/ac6e43

Giommi, P., Brandt, C. H., Barres de Almeida, U., et al. 2019, A&A, 631, A116, doi: 10.1051/0004-6361/201935646

Glennie, A., Jonker, P. G., Fender, R. P., Nagayama, T., & Pretorius, M. L. 2015, Monthly Notices of the Royal Astronomical Society, 450, 3765–3770, doi: 10.1093/mnras/stv801

Greiner, J., Voges, W., Boller, T., & Hartmann, D. 1999, A&AS, 138, 441, doi: 10.1051/aas:1999300

Haberl, F., Geppert, U., Aschenbach, B., & Hasinger, G. 2006, A&A, 460, 811, doi: 10.1051/0004-6361:20066198

Haberl, F., & Sturm, R. 2016, A&A, 586, A81, doi: 10.1051/0004-6361/201527326

Hachisu, I., & Kato, M. 2018, ApJS, 237, 4, doi: 10.3847/1538-4365/aac833

Hajela, A., Margutti, R., Alexander, K. D., et al. 2019, ApJL, 886, L17, doi: 10.3847/2041-8213/ab5226

Hajela, A., Margutti, R., Kathirgamaraju, A., et al. 2020, Research Notes of the American Astronomical Society, 4, 68, doi: 10.3847/2515-5172/ab9229

Hameury, J. M., Barret, D., Lasota, J. P., et al. 2003, A&A, 399, 631, doi: 10.1051/0004-6361:20021746

Hancock, P. J., Anderson, G. E., Williams, A., et al. 2019, PASA, 36, e046, doi: 10.1017/pasa.2019.40

Harris, C. R., Millman, K. J., van der Walt, S. J., et al. 2020, Nature, 585, 357, doi: 10.1038/s41586-020-2649-2

Heng, K., Haberl, F., Aschenbach, B., & Hasinger, G. 2008, ApJ, 676, 361, doi: 10.1086/526517

Ho, A. Y. Q., Perley, D. A., Gal-Yam, A., et al. 2021, arXiv e-prints, arXiv:2105.08811. https://arxiv.org/abs/2105.08811

Ho, A. Y. Q., Margalit, B., Bremer, M., et al. 2022, ApJ, 932, 116, doi: 10.3847/1538-4357/ac4e97

Holoien, T. W. S., Brown, J. S., Auchettl, K., et al. 2018, MNRAS, 480, 5689, doi: 10.1093/mnras/sty2273

Holoien, T. W. S., Prieto, J. L., Bersier, D., et al. 2014, MNRAS, 445, 3263, doi: 10.1093/mnras/stu1922

Holoien, T. W. S., Vallely, P. J., Auchettl, K., et al. 2019, ApJ, 883, 111, doi: 10.3847/1538-4357/ab3c66

Hunter, J. D. 2007, Computing in Science & Engineering, 9, 90, doi: 10.1109/MCSE.2007.55

Immler, S. 2010, The Astronomer's Telegram, 2478, 1

Immler, S., Brown, P. J., Filippenko, A. V., & Pooley, D. 2007a, The Astronomer's Telegram, 1290, 1

Immler, S., Li, B., Yang, Y., & Wilson, A. 2007b, Central Bureau Electronic Telegrams, 828, 1

Immler, S., Milne, P., & Pooley, D. 2010, The Astronomer's Telegram, 3012, 1

Immler, S., & Pooley, D. 2007, The Astronomer's Telegram, 1004, 1

Immler, S., Pooley, D., & Brown, P. J. 2007c, The Astronomer's Telegram, 981, 1

Immler, S., Pooley, D., Brown, P. J., Li, W., & Filippenko, A. V. 2007d, The Astronomer's Telegram, 1284, 1

Immler, S., Pooley, D., Brown, P. J., & Milne, P. 2009, The Astronomer's Telegram, 1918, 1

Immler, S., & Russell, B. R. 2009, The Astronomer's Telegram, 2111, 1

Immler, S., Brown, P. J., Milne, P., et al. 2007e, ApJ, 664, 435, doi: 10.1086/518466

Immler, S., Modjaz, M., Landsman, W., et al. 2008, ApJL, 674, L85, doi: 10.1086/529373

in't Zand, J. J. M. 2005, A&A, 441, L1, doi: 10.1051/0004-6361:200500162

Israel, G. L., Romano, P., Mangano, V., et al. 2008, ApJ, 685, 1114, doi: 10.1086/590486

Jacobson-Galán, W. V., Margutti, R., Kilpatrick, C. D., et al. 2020, ApJ, 898, 166, doi: 10.3847/1538-4357/ab9e66

Jacobson-Galán, W. V., Venkatraman, P., Margutti, R., et al. 2022, ApJ, 932, 58, doi: 10.3847/1538-4357/ac67dc

Jonker, P. G., Miller-Jones, J. C. A., Homan, J., et al. 2012, MNRAS, 423, 3308, doi: 10.1111/j.1365-2966.2012.21116.x

Jonker, P. G., Glennie, A., Heida, M., et al. 2013, The Astrophysical Journal, 779, 14, doi: 10.1088/0004-637x/779/1/14

Kantharia, N. G. 2017, arXiv e-prints, arXiv:1703.04087. https://arxiv.org/abs/1703.04087

Koliopanos, F., & Vasilopoulos, G. 2018, A&A, 614, A23, doi: 10.1051/0004-6361/201731623

Komossa, S. 2015, Journal of High Energy Astrophysics, 7, 148, doi: 10.1016/j.jheap.2015.04.006

Kong, A. K. H., Kuulkers, E., Charles, P. A., & Homer, L. 2000, MNRAS, 312, L49, doi: 10.1046/j.1365-8711.2000.03334.x

Kouveliotou, C., Meegan, C. A., Fishman, G. J., et al. 1993, ApJL, 413, L101, doi: 10.1086/186969

Kouveliotou, C., Woosley, S. E., Patel, S. K., et al. 2004, ApJ, 608, 872, doi: 10.1086/420878

Kulkarni, S. R. 2012, arXiv e-prints, arXiv:1202.2381. https://arxiv.org/abs/1202.2381

La Palombara, N., & Mereghetti, S. 2007, A&A, 474, 137, doi: 10.1051/0004-6361:20077970

Levan, A. J., Tanvir, N. R., Starling, R. L. C., et al. 2014, ApJ, 781, 13, doi: 10.1088/0004-637X/781/1/13

Leyder, J. C., Walter, R., Lazos, M., Masetti, N., & Produit, N. 2007, A&A, 465, L35, doi: 10.1051/0004-6361:20066317

Li, C. K., Lin, L., Xiong, S. L., et al. 2021, Nature Astronomy, 5, 378, doi: 10.1038/s41550-021-01302-6

Li, K.-L., Hambsch, F.-J., Munari, U., et al. 2020a, ApJ, 905, 114, doi: 10.3847/1538-4357/abc3be

Li, X., Li, X., Tan, Y., et al. 2020b, Journal of High Energy Astrophysics, 27, 64, doi: 10.1016/j.jheap.2020.02.009

Linford, J. D., Chomiuk, L., Nelson, T., et al. 2017, ApJ, 842, 73, doi: 10.3847/1538-4357/aa7512

López-Navas, E., Degenaar, N., Parikh, A. S., Hernández Santisteban, J. V., & van den Eijnden, J. 2020, MNRAS, 493, 940, doi: 10.1093/mnras/staa275

Lorimer, D. R., Bailes, M., McLaughlin, M. A., Narkevic, D. J., & Crawford, F. 2007, Science, 318, 777, doi: 10.1126/science.1147532

Lutovinov, A. A., Tsygankov, S. S., Krivonos, R. A., Molkov, S. V., & Poutanen, J. 2017, ApJ, 834, 209, doi: 10.3847/1538-4357/834/2/209

Maitra, C., Haberl, F., Vasilopoulos, G., et al. 2021, A&A, 647, A8, doi: 10.1051/0004-6361/202039468

Mangano, V., Burrows, D. N., Sbarufatti, B., & Cannizzo, J. K. 2016, ApJ, 817, 103, doi: 10.3847/0004-637X/817/2/103

Margutti, R., & Chornock, R. 2021, ARA&A, 59, doi: 10.1146/annurev-astro-112420-030742

Margutti, R., Soderberg, A., & Milisavljevic, D. 2013, The Astronomer's Telegram, 5106, 1

Margutti, R., Metzger, B. D., Chornock, R., et al. 2017, ApJ, 836, 25, doi: 10.3847/1538-4357/836/1/25

Margutti, R., Chornock, R., Metzger, B. D., et al. 2018, ApJ, 864, 45, doi: 10.3847/1538-4357/aad2df

Margutti, R., Metzger, B. D., Chornock, R., et al. 2019, The Astrophysical Journal, 872, 18, doi: 10.3847/1538-4357/aafa01

Matsuoka, M., Kawasaki, K., Ueno, S., et al. 2009, PASJ, 61, 999, doi: 10.1093/pasj/61.5.999

Matthews, D., Brethauer, D., Margutti, R., et al. 2022, Transient Name Server AstroNote, 218, 1

Maxwell, J. E., Lugger, P. M., Cohn, H. N., et al. 2012, ApJ, 756, 147, doi: 10.1088/0004-637X/756/2/147

Mazzali, P. A., Valenti, S., Della Valle, M., et al. 2008, Science, 321, 1185, doi: 10.1126/science.1158088

McGowan, K. E., Priedhorsky, W. C., & Trudolyubov, S. P. 2004, ApJ, 601, 1100, doi: 10.1086/380758

Meidinger, N. 2018, Contributions of the Astronomical Observatory Skalnate Pleso, 48, 498. https://arxiv.org/abs/1702.01079

Mereghetti, S., Savchenko, V., Ferrigno, C., et al. 2020, ApJL, 898, L29, doi: 10.3847/2041-8213/aba2cf

Merloni, A., Predehl, P., Becker, W., et al. 2012, arXiv e-prints, arXiv:1209.3114. https://arxiv.org/abs/1209.3114

Metzger, B. D., Williams, P. K. G., & Berger, E. 2015, ApJ, 806, 224, doi: 10.1088/0004-637X/806/2/224

Middleton, M. J., Miller-Jones, J. C. A., Markoff, S., et al. 2013, Nature, 493, 187, doi: 10.1038/nature11697

Miller, J. M., Kaastra, J. S., Miller, M. C., et al. 2015, Nature, 526, 542, doi: 10.1038/nature15708

Miniutti, G., Saxton, R. D., Giustini, M., et al. 2019, Nature, 573, 381, doi: 10.1038/s41586-019-1556-x

Misra, K., Pooley, D., Chandra, P., et al. 2007, MNRAS, 381, 280, doi: 10.1111/j.1365-2966.2007.12258.x

Miura, J., Tsujimoto, M., Tsuboi, Y., et al. 2008, PASJ, 60, S49, doi: 10.1093/pasj/60.sp1.S49

Mong, Y.-L., & Ng, C.-Y. 2018, The Astrophysical Journal, 852, 86, doi: 10.3847/1538-4357/aa9e90

Mukai, K. 1993, Legacy, 3, 21

—. 2017, PASP, 129, 062001, doi: 10.1088/1538-3873/aa6736

Mukai, K., Orio, M., & Della Valle, M. 2008, ApJ, 677, 1248, doi: 10.1086/529362

Munari, U., Ribeiro, V. A. R. M., Bode, M. F., & Saguner, T. 2011, MNRAS, 410, 525, doi: 10.1111/j.1365-2966.2010.17462.x

Mushotzky, R. 2018, in Society of Photo-Optical Instrumentation Engineers (SPIE) Conference Series, Vol. 10699, Space Telescopes and Instrumentation 2018: Ultraviolet to Gamma Ray, ed. J.-W. A. den Herder, S. Nikzad, & K. Nakazawa, 1069929, doi: 10.1117/12.2310003

Nakar, E. 2020, PhR, 886, 1, doi: 10.1016/j.physrep.2020.08.008

Nakar, E., & Sari, R. 2010, ApJ, 725, 904, doi: 10.1088/0004-637X/725/1/904

—. 2012, ApJ, 747, 88, doi: 10.1088/0004-637X/747/2/88

Neustroev, V. V., Page, K. L., Kuulkers, E., et al. 2018, A&A, 611, A13, doi: 10.1051/0004-6361/201731719

Novara, G., Esposito, P., Tiengo, A., et al. 2020, ApJ, 898, 37, doi: 10.3847/1538-4357/ab98f8

O'Brien, P. T., & Smartt, S. J. 2013, Philosophical Transactions of the Royal Society of London Series A, 371, 20120498, doi: 10.1098/rsta.2012.0498

Olausen, S. A., & Kaspi, V. M. 2014, The Astrophysical Journal Supplement Series, 212, 6, doi: 10.1088/0067-0049/212/1/6

Page, K. L., Beardmore, A. P., & Osborne, J. P. 2020, Advances in Space Research, 66, 1169, doi: 10.1016/j.asr.2019.08.003

Pala, A. F., Gänsicke, B. T., Breedt, E., et al. 2020, MNRAS, 494, 3799, doi: 10.1093/mnras/staa764

pandas development team, T. 2020, pandas-dev/pandas: Pandas, 1.1.3, Zenodo, doi: 10.5281/zenodo.4067057

Pedregosa, F., Varoquaux, G., Gramfort, A., et al. 2011, Journal of Machine Learning Research, 12, 2825

Petroff, E., Hessels, J. W. T., & Lorimer, D. R. 2019, A&A Rv, 27, 4, doi: 10.1007/s00159-019-0116-6

—. 2022, A&A Rv, 30, 2, doi: 10.1007/s00159-022-00139-w

Pian, E., Amati, L., Antonelli, L. A., et al. 2000, ApJ, 536, 778, doi: 10.1086/308978

Pietka, M., Fender, R. P., & Keane, E. F. 2015, MNRAS, 446, 3687, doi: 10.1093/mnras/stu2335

Pietrzyński, G., Graczyk, D., Gieren, W., et al. 2013, Nature, 495, 76, doi: 10.1038/nature11878

Pleunis, Z., Good, D. C., Kaspi, V. M., et al. 2021, ApJ, 923, 1, doi: 10.3847/1538-4357/ac33ac

Poggiani, R. 2009, NewA, 14, 4, doi: 10.1016/j.newast.2008.04.004

Pooley, D., Immler, S., & Filippenko, A. V. 2007, The Astronomer's Telegram, 1023, 1

Pooley, D., & Lewin, W. H. G. 2002, IAUC, 8024, 2

—. 2003, The Astronomer's Telegram, 116, 1

—. 2004a, IAUC, 8323, 2

—. 2004b, IAUC, 8390, 1

Pooley, D., Lewin, W. H. G., Fox, D. W., et al. 2002, ApJ, 572, 932, doi: 10.1086/340346

Pursiainen, M., Childress, M., Smith, M., et al. 2018, MNRAS, 481, 894, doi: 10.1093/mnras/sty2309

Pye, J. P., Rosen, S., Fyfe, D., & Schröder, A. C. 2015, A&A, 581, A28, doi: 10.1051/0004-6361/201526217

Qiu, Y., Soria, R., Wang, S., et al. 2019, ApJ, 877, 57, doi: 10.3847/1538-4357/ab16e7

Quirola-Vásquez, J., Bauer, F. E., Jonker, P. G., et al. 2022, A&A, 663, A168, doi: 10.1051/0004-6361/202243047

Raj, A., Banerjee, D. P. K., & Ashok, N. M. 2013, MNRAS, 433, 2657, doi: 10.1093/mnras/stt946

Raj, A., Ashok, N. M., Rudy, R. J., et al. 2015, AJ, 149, 136, doi: 10.1088/0004-6256/149/4/136

Ray, P. S., Arzoumanian, Z., Ballantyne, D., et al. 2019, arXiv e-prints, arXiv:1903.03035. https://arxiv.org/abs/1903.03035

Rea, N., Borghese, A., Esposito, P., et al. 2016, ApJL, 828, L13, doi: 10.3847/2041-8205/828/1/L13

Rea, N., Esposito, P., Pons, J. A., et al. 2013, ApJL, 775, L34, doi: 10.1088/2041-8205/775/2/L34

Reig, P. 2011, Ap&SS, 332, 1, doi: 10.1007/s10509-010-0575-8

Rivera Sandoval, L. E., Maccarone, T. J., Corsi, A., et al. 2018, MNRAS, 480, L146, doi: 10.1093/mnrasl/sly145

—. 2019, MNRAS, 484, L7, doi: 10.1093/mnrasl/sly235

Rohatgi, A. 2019, WebPlotDigitizer (4.2), https://automeris.io/WebPlotDigitizer

Roming, P. W. A., Pritchard, T. A., Brown, P. J., et al. 2009, ApJL, 704, L118, doi: 10.1088/0004-637X/704/2/L118

Rouco Escorial, A., Fong, W.-f., Berger, E., et al. 2022, arXiv e-prints, arXiv:2210.05695. https://arxiv.org/abs/2210.05695

Russell, B. R., & Immler, S. 2010, The Astronomer's Telegram, 2389, 1

Russell, B. R., Immler, S., & Milne, P. 2010, The Astronomer's Telegram, 2618, 1

Russell, T. D., Miller-Jones, J. C. A., Sivakoff, G. R., et al. 2016, MNRAS, 460, 3720, doi: 10.1093/mnras/stw1238

Sakano, M., Koyama, K., Murakami, H., Maeda, Y., & Yamauchi, S. 2002, ApJS, 138, 19, doi: 10.1086/324020

Sazonov, S. Y., Lutovinov, A. A., & Sunyaev, R. A. 2004, Nature, 430, 646, doi: 10.1038/nature02748

Schaefer, B. E. 2010, ApJS, 187, 275, doi: 10.1088/0067-0049/187/2/275

—. 2018, MNRAS, 481, 3033, doi: 10.1093/mnras/sty2388

Schlegel, E. M. 2001, ApJL, 556, L25, doi: 10.1086/322269

Schlegel, E. M., & Ryder, S. 2002, IAUC, 7913, 1

Schulze, S., Ho, A. Y. Q., Perley, D. A., Yan, L., & Fremling, C. 2022, Transient Name Server AstroNote, 207, 1

Sidoli, L., Romano, P., Mangano, V., et al. 2008, ApJ, 687, 1230, doi: 10.1086/590077

Soderberg, A., Grindlay, J. E., Bloom, J. S., et al. 2009, in astro2010: The Astronomy and Astrophysics Decadal Survey, Vol. 2010, 278. https://arxiv.org/abs/0902.012674

Soderberg, A. M., Chevalier, R. A., Kulkarni, S. R., & Frail, D. A. 2006, ApJ, 651, 1005, doi: 10.1086/507571

Soderberg, A. M., Berger, E., Page, K. L., et al. 2008, Nature, 453, 469, doi: 10.1038/nature06997

Soderberg, A. M., Margutti, R., Zauderer, B. A., et al. 2012, ApJ, 752, 78, doi: 10.1088/0004-637X/752/2/78

Soria, R., & Perna, R. 2008, ApJ, 683, 767, doi: 10.1086/589995

Soria, R., Pian, E., & Mazzali, P. A. 2004, A&A, 413, 107, doi: 10.1051/0004-6361:20031506

Staley, T. D., Titterington, D. J., Fender, R. P., et al. 2013, MNRAS, 428, 3114, doi: 10.1093/mnras/sts259

Stone, N. C., & Metzger, B. D. 2016, MNRAS, 455, 859, doi: 10.1093/mnras/stv2281

Sturm, R., Haberl, F., Aschenbach, B., & Hasinger, G. 2010, A&A, 515, A5, doi: 10.1051/0004-6361/200913317

Sugawara, Y., Nakahira, S., Negoro, H., et al. 2020, GRB Coordinates Network, 27661, 1

Sugizaki, M. 2010, in The First Year of MAXI: Monitoring Variable X-ray Sources, 14

Svirski, G., & Nakar, E. 2014, ApJL, 788, L14, doi: 10.1088/2041-8205/788/1/L14

Tanaka, M., Tominaga, N., Morokuma, T., et al. 2016, ApJ, 819, 5, doi: 10.3847/0004-637X/819/1/5

Tetarenko, B. E., Sivakoff, G. R., Heinke, C. O., & Gladstone, J. C. 2016, ApJS, 222, 15, doi: 10.3847/0067-0049/222/2/15

The CHIME/FRB Collaboration, Andersen, B. Â. C., Bandura, K. Â. M., Bhardwaj, M., et al. 2020, Nature, 587, 54, doi: 10.1038/s41586-020-2863-y

The Lynx Team. 2019, Lynx X-ray Observatory Concept Study Report, Tech. rep., Lynx Observatory

Tozzi, P., Gilli, R., Mainieri, V., et al. 2006, A&A, 451, 457, doi: 10.1051/0004-6361:20042592

Tsuboi, Y., Yamazaki, K., Sugawara, Y., et al. 2016, PASJ, 68, 90, doi: 10.1093/pasj/psw081

Tsunemi, H., Tomida, H., Katayama, H., et al. 2010, Publications of the Astronomical Society of Japan, 62, 1371, doi: 10.1093/pasj/62.6.1371

Vasilopoulos, G., Haberl, F., & Maggi, P. 2017a, MNRAS, 470, 1971, doi: 10.1093/mnras/stx1359

Vasilopoulos, G., Haberl, F., Sturm, R., Maggi, P., & Udalski, A. 2014, A&A, 567, A129, doi: 10.1051/0004-6361/201423934

Vasilopoulos, G., Lander, S. K., Koliopanos, F., & Bailyn, C. D. 2020a, MNRAS, 491, 4949, doi: 10.1093/mnras/stz3298

Vasilopoulos, G., Maitra, C., Haberl, F., Hatzidimitriou, D., & Petropoulou, M. 2018, MNRAS, 475, 220, doi: 10.1093/mnras/stx3139

Vasilopoulos, G., Zezas, A., Antoniou, V., & Haberl, F. 2017b, MNRAS, 470, 4354, doi: 10.1093/mnras/stx1507

Vasilopoulos, G., Ray, P. S., Gendreau, K. C., et al. 2020b, MNRAS, 494, 5350, doi: 10.1093/mnras/staa991

Villar, V. A., Berger, E., Metzger, B. D., & Guillochon, J. 2017, ApJ, 849, 70, doi: 10.3847/1538-4357/aa8fcb

Virtanen, P., Gommers, R., Oliphant, T. E., et al. 2020, Nature Methods, 17, 261, doi: 10.1038/s41592-019-0686-2

Wang, C. W., Xiong, S. L., Zhang, Y. Q., et al. 2022, The Astronomer's Telegram, 15682, 1

Watson, D., Hjorth, J., Levan, A., et al. 2004, ApJL, 605, L101, doi: 10.1086/420844

Watson, M. G., Auguères, J. L., Ballet, J., et al. 2001, A&A, 365, L51, doi: 10.1051/0004-6361:20000067

Wei, J., Cordier, B., Antier, S., et al. 2016, arXiv e-prints, arXiv:1610.06892. https://arxiv.org/abs/1610.06892

Wes McKinney. 2010, in Proceedings of the 9th Python in Science Conference, ed. Stéfan van der Walt & Jarrod Millman, 56 – 61, doi: 10.25080/Majora-92bf1922-00a

Wheatley, P. J., Mauche, C. W., & Mattei, J. A. 2003, MNRAS, 345, 49, doi: 10.1046/j.1365-8711.2003.06936.x

Wilson-Hodge, C. A., Malacaria, C., Jenke, P. A., et al. 2018, ApJ, 863, 9, doi: 10.3847/1538-4357/aace60

Worpel, H., Schwope, A. D., Traulsen, I., Mukai, K., & Ok, S. 2020, A&A, 639, A17, doi: 10.1051/0004-6361/202038038

Yao, Y., Ho, A. Y. Q., Medvedev, P., et al. 2022, ApJ, 934, 104, doi: 10.3847/1538-4357/ac7a41

Yuan, W. 2017, in 7 years of MAXI: monitoring X-ray Transients, ed. M. Serino, M. Shidatsu, W. Iwakiri, & T. Mihara, 247

Zampieri, L., Mucciarelli, P., Pastorello, A., et al. 2005, MNRAS, 364, 1419, doi: 10.1111/j.1365-2966.2005.09671.x

Zhang, S., Santangelo, A., Feroci, M., et al. 2019, Science China Physics, Mechanics, and Astronomy, 62, 29502, doi: 10.1007/s11433-018-9309-2